ELSEVIER

Increased extreme fire weather occurrence in southeast Australia and related atmospheric drivers

Doug Richardson [a,*], Amanda S. Black [a], Didier P. Monselesan [a], James S. Risbey [a], Dougal T. Squire [a], Carly R. Tozer [a], Josep G. Canadell [b]

[a] *Climate Science Centre, CSIRO Oceans & Atmosphere, Hobart, Tasmania, Australia*
[b] *Climate Science Centre, CSIRO Oceans & Atmosphere, Canberra, ACT, Australia*

ARTICLE INFO

ABSTRACT

There is evidence suggesting that fire activity in southeast Australia has increased in the past two decades. There is also anecdotal evidence that pyrocumulonimbus events have become more common, although the observed record is short. We explore the extent to which possible changes in fire and pyrocumulonimbus occurrence in southeast Australia can be explained by changes in the number of extreme (above the 95th percentile) days per year of two fire-weather indices, the Forest Fire Danger Index (FFDI) and the continuous Haines index (C-Haines). For the period 1958 through 2020, we show that there is a dependence between the number of extreme FFDI days per year and burned area for forested parts of southeast Australia. To a lesser extent, there is a relationship between the FFDI and pyrocumulonimbus occurrences. We find an increase in the occurrence of extreme FFDI days from the late 1990s, with up to 24 more extreme days per year. In the southwest of the state of Victoria, there are concomitant increases in temperature and wind speed, and decreases in relative humidity. We show that the structure of C-Haines has not changed, but extreme days more frequently coincide with extreme FFDI days. This suggests that possible observed increases in pyrocumulonimbus occurrences may partly be explained as a consequence of the increases in co-occurring extreme FFDI and C-Haines days, rather than due to changes in the atmospheric stability. We also find that changes in the atmospheric circulation are consistent with those seen in the fire weather indices. Increased surface and mid-tropospheric pressure since 1998 are consistent with a poleward shift of the storm track. In particular, an increase in anticyclonic anomalies in the Tasman Sea is indicative of enhanced blocking activity. Although blocking frequency in these longitudes has decreased overall, the proportion of extreme FFDI days that are considered blocked has increased.

1. Introduction

For much of Australia, particularly the sparsely-populated tropical savannas of the North, vegetation fires are characterised by their high frequency of occurrence and low intensity. Highly populated urban centres in the coastal southeast and southwest, however, are generally co-located with eucalypt forest, which tends to burn less frequently but at potentially very high intensities (Russell-Smith et al., 2007; Bradstock, 2010; Murphy et al., 2013). As a result, fires can have devastating socio-economic, as well as environmental, impact (e.g. Gill et al., 2013; Moritz et al., 2014; Ward et al., 2020).

Since the early 2000s, several very large-scale fires have occurred in southeast Australia, notably during the 2002-03, 2006-07, 2008-09 and 2019-20 fire seasons. This raises the question of whether fire activity has increased in recent decades. Data limitations, such as short observational records and changes in spatial coverage, challenge analyses of

long term changes in fire activity. Nevertheless, relative to the preceding few decades, there are indications that the rate of fire occurrence in southeast Australia changed in the early 2000s. Since then, there has been shorter intervals between large-scale fires (Fairman et al., 2016; Sharples et al., 2016; Lindenmayer and Taylor, 2020; Abram et al., 2021; Canadell et al., 2021). This prevents the regeneration of vegetation that is otherwise adaptable (Fairman et al., 2019). The 2019-20 'Black Summer' was the third fire season (July through June) to burn over one million hectares in the state of Victoria since 2003, a feat not achieved by any fire since at least 1950 (Lindenmayer and Taylor, 2020). Those three so-called 'megafires' contributed to a statistically significant increase in burned area for the 2003–2020 period compared to 1950–2002 (Lindenmayer and Taylor, 2020). Furthermore, Canadell et al. (2021) showed a marked increase in the number of years with a

---

* Corresponding author.
E-mail address: doug.richardson@csiro.au (D. Richardson).

large burned area since around the year 2000, evident from 32 years of satellite data and from 90 years of fire histories collated from Australian State and Territory agencies.

Under the right conditions, large and intense fires can generate pyrocumulonimbus (thunderstorms that form in the convective plume of a fire). They present a particularly difficult challenge to firefighters as they are very unpredictable, capable of enhancing a fire's intensity and speed of spread, and of spotting (igniting) new fires through ember transport or lightning strikes (e.g. Dowdy et al., 2017). Pyrocumulonimbus occurrences are identified using expert analysis of local and remote (e.g. satellite) sources (Di Virgilio et al., 2019). The vast majority of identified events in Australia have occurred since 2000 (Di Virgilio et al., 2019). However, data prior to 1998 should be treated cautiously, as potential pyrocumulonimbus events prior to this have to be confirmed retrospectively (Sharples et al., 2016).

Due to this short observational record, it is not possible to describe long-term trends in pyrocumulonimbus. Nevertheless, anecdotal evidence from fire agencies suggests these events have become more frequent (Readfearn, 2019), while the 2019-20 fire season experienced a record 29 occurrences (Abram et al., 2021). This is over one-third of the number identified over the entire period from the late 1970s to April 2019 (82 events; McRae et al., 2015; Sharples et al., 2016; Di Virgilio et al., 2019). Increases in the number of pyrocumulonimbus occurrences would be consistent with physical changes in the lower to mid-troposphere, which show that conditions favourable for pyrocumulonimbus have become more common, a trend that is projected to continue into future decades (Dowdy and Pepler, 2018; Dowdy et al., 2019). Furthermore, as intense fires are a prerequisite for pyrocumulonimbus development (McRae et al., 2015; Tory and Thurston, 2015), increases in fire occurrence or intensity would be expected to result in more frequent pyrocumulonimbus.

There are various complex processes that could contribute to changes in fire occurrence, such as the set-up of atmospheric conditions conducive to fire development (Voice and Gauntlett, 1984; Mills, 2005a,b; Bradstock, 2010; Sharples et al., 2010; Engel et al., 2013; Bradstock et al., 2014; Reeder et al., 2015; Fiddes et al., 2016), or changes in fuel accumulation due to management practices or environmental factors (Bradstock, 2010; Lindenmayer et al., 2020). We focus on one contributor to fire: the associated weather conditions ('fire weather'). In Australia, fire weather is typically monitored using the McArthur Forest Fire Danger Index (FFDI; Luke and McArthur, 1978; Noble et al., 1980), which combines temperature, relative humidity, wind speed and an estimate of drought. As a purely meteorological index, the FFDI does not account for other factors critical to fire activity, such as fuel type and availability. Despite this, it has proved a useful predictor of fire and its impacts (Blanchi et al., 2010; Harris et al., 2012; Blanchi et al., 2014; Tolhurst and McCarthy, 2016; Abram et al., 2021; Canadell et al., 2021).

A key measure of pyrocumulonimbus potential is the continuous Haines index (C-Haines; Haines, 1988; Mills and McCaw, 2010), which attempts to characterise atmospheric humidity and vertical stability. The atmospheric stability can have a strong influence on potential pyroconvection, including pyrocumulonimbus (Haines, 1988; Mills and McCaw, 2010). C-Haines has therefore emerged as an important meteorological indicator of the potential for pyrocumulonimbus (Mills and McCaw, 2010; Fromm et al., 2012; Dowdy and Pepler, 2018; Dowdy et al., 2019). However, C-Haines does not account for any of the other processes also important for pyrocumulonimbus development, such as the presence of a fire or the type of terrain or fuel (e.g. McRae et al., 2015; Tory and Thurston, 2015; Di Virgilio et al., 2019).

Numerous studies have investigated the long-term changes in the FFDI and C-Haines. The general consensus is that recent decades feature a greater prevalence and severity of days with weather conducive to fire and pyrocumulonimbus, together with such days now occurring over a longer fire season, particularly in southeast Australia (Clarke et al., 2013; Bradstock et al., 2014; Jolly et al., 2015; Sharples et al., 2016; Dowdy, 2018; Dowdy and Pepler, 2018; Harris and Lucas, 2019; Abram et al., 2021; Canadell et al., 2021). Increases in the FFDI in this region are associated with increases in temperature and decreases in precipitation and humidity (Bradstock et al., 2014; Jolly et al., 2015; Abram et al., 2021). Changes in large-scale teleconnection modes may also play a role. The El Niño Southern Oscillation, the Indian Ocean Dipole (IOD) and the Southern Annular Mode (SAM) have been associated with Australian fire and fire weather variability (e.g. Cai et al., 2009a; Harris and Lucas, 2019; Abram et al., 2021). Evidence suggests the IOD and the SAM have trended towards more frequent occurrences of their fire-promoting states (Arblaster and Meehl, 2006; Cai et al., 2009b; Thompson et al., 2011; Cai et al., 2013; Abram et al., 2020).

To complement studies that relate changes in fire weather and large-scale climate modes, we present an analysis of changes in fire weather and the associated atmospheric circulation, focusing on synoptic-scale dynamics such as the storm track and blocking. We utilise statistical step-change methods to identify suitable periods over which to split our data. Differences between these periods are used to quantify changes in local meteorological variables and the atmospheric circulation. Applying step change tests to Australian fire weather indices in this way is novel, and provides a useful point of comparison with studies that analyse changes in other ways, for example by fitting linear trends (Clarke et al., 2013; Jolly et al., 2015; Harris and Lucas, 2019; Canadell et al., 2021) or by splitting the data at an arbitrary point in time (Dowdy, 2018; Dowdy and Pepler, 2018).

This article is organised as follows. In Section 2, we detail the calculation of the FFDI and C-Haines, set out our criteria for identifying step changes in fire weather, describe a suite of atmospheric circulation diagnostics, and introduce observed fire and pyrocumulonimbus datasets. We report the results of our analysis in Section 3, covering the relationships between fire, pyrocumulonimbus events and fire weather, and changes in fire weather, surface conditions and the atmospheric circulation. Finally, we provide a discussion and conclusions in Section 4.

2. Data and methodology

2.1. Fire weather indices

We calculate the daily McArthur Forest Fire Danger Index (FFDI; Luke and McArthur, 1978; Noble et al., 1980) for the period 1958 through October 2020 over Australia. The FFDI is computed using the following formula:

$$\text{FFDI} = D^{0.987} \exp(0.0338T - 0.0345H + 0.0234\,W + 0.243147). \quad (1)$$

We use the Japanese 55-year reanalysis (JRA55; Japan Meteorological Agency, 2013), with a spatial resolution of $1.25°$ latitude and longitude and a six-hourly temporal resolution. We use 0600 UTC (mid-afternoon in Australia) data for 2 m temperature, T (°C), 2 m relative humidity, H (%), and 10 m wind speed, W (km/h). The drought factor, D, is the accumulated 20-day precipitation scaled to range between 0 and 10, with larger D for lower precipitation totals.

Our FFDI differs from other studies in two ways. First, some studies calculate the FFDI using observation data where possible, rather than a reanalysis (e.g. Dowdy, 2018; Dowdy and Pepler, 2018). We use reanalysis data for the FFDI to ensure dynamical consistency in our analysis. The C-Haines requires input variables typically only available from climate models, and so is calculated with reanalysis data. Furthermore, part of our study will investigate changes in the atmospheric circulation associated with changes in fire weather indices. Given the need for a reanalysis product for a substantial part of our analysis, we prioritise dynamical consistency over using a product closer to observations for calculating the FFDI. The downside of this is that reanalysis products vary depending on, for example, the model and data assimilation scheme. Our results, then, may be sensitive to the

choice of reanalysis used to derive the indices herein. However, JRA55 is comparable with other reanalyses, including recent products such as ERA5, for the key variables required here such as 2 m temperature and relative humidity (Kobayashi et al., 2015; Harada et al., 2016; Simmons et al., 2021).

Second, our formulation of the drought factor is simpler than the usual approach, which typically estimates soil moisture using precipitation and temperature with a series of empirical equations (e.g. Finkele et al., 2006). By calculating a number of long-term statistics (i.e. those most important to our study), we find our FFDI consistent with those presented in other studies (Dowdy, 2018; Dowdy and Pepler, 2018). In particular, we were able to faithfully reproduce figures from those studies of the spatial and seasonal variability, and of the differences in mean and extreme FFDI days between various periods. Further information and two figures are provided in the supplementary material.

Pyrocumulonimbus potential is measured using the continuous Haines index (C-Haines; Haines, 1988; Mills and McCaw, 2010), which is calculated using JRA55 0600 UTC values of the temperature at 850 hPa (T_{850}), the temperature at 700 hPa (T_{700}), and the dew point depression at 850 hPa (DD_{850}), all measured in degrees Celsius. The index is a combination of estimates of the vertical column atmospheric stability

$$C_a = \frac{T_{850} - T_{700} - 4}{2}, \tag{2}$$

and the humidity in the lower troposphere

$$C_b = \frac{\max(DD_{850}, 30) - 3}{3}. \tag{3}$$

If $C_b > 5$ then set $C_b = (C_b - 5)/2 + 5$. The C-Haines index is defined as $C = C_a + C_b$. Reanalysis data are commonly used to derive the C-Haines index (Dowdy and Pepler, 2018; Dowdy et al., 2019).

We define an extreme FFDI or C-Haines event as when the index is above the 95th percentile of the 1958–2019 climatology. Adopting a percentile-based definition in this context is common as the range of values the indices can take may vary spatially or according to the dataset used for their calculation (e.g. Dowdy, 2018; Dowdy and Pepler, 2018; Plucinski et al., 2020). Furthermore, numerical thresholds, such as those designed for operational use, are perhaps not well suited for reanalysis data because of the strong dependence on spatial resolution. A numerical threshold is used for operational fire danger rating purposes across Australia, for which 'extreme' equates to an FFDI of 75 or greater. A recent study showed that for six study areas in southern Australia between 2002 and 2016, the FFDI exceeded a value of 50 (the 'severe' category) on less than one percent of days (Plucinski et al., 2020). Extreme FFDI days in this study are therefore much more frequent than 'extreme' days as defined for official fire danger rating purposes.

The statistic we use to measure changes in extreme fire weather is the yearly totals of extreme index occurrences. We consider a year as running from July through June of the following calendar year to span the southern Australia fire season. We use the earlier of the two calendar years to indicate which period is under discussion. For example, '2019' refers to the period July 2019 through June 2020.

2.2. Identifying step changes in fire weather

To identify possible step changes, we use the Pettitt test (Pettitt, 1979), which is a widely used non-parametric test to assess the presence of potential abrupt changes in the mean or median of a time series (e.g. Bárdossy and Caspary, 1990; Busuioc and von Storch, 1996; Wijngaard et al., 2003; Villarini et al., 2009; Ferguson and Villarini, 2012). Following Pettitt (1979), a set of independent and identically distributed random variables $X_1, X_2, \ldots, X_T$ is said to have a change point at τ if X_t for $t = 1, \ldots, \tau$ have a common distribution function $F_1(x)$, and X_t for $t = \tau + 1, \ldots, T$ have a common distribution function $F_2(x)$, and $F_1(x) \neq F_2(x)$. The null hypothesis of 'no change', $H_0 : \tau = T$,

is tested against the alternative hypothesis of 'change', $H_1 : 1 \leq \tau < T$, using the statistic

$$K_T = \max_{1 \leq t < T} |U_{t,T}|, \tag{4}$$

where

$$U_{t,T} = \sum_{i=1}^{t} \sum_{j=i+1}^{T} \text{sgn}(X_i - X_j). \tag{5}$$

We attempt to mitigate the effects of autocorrelation by applying a block bootstrap procedure (Kunsch, 1989; Lahiri, 2003; Wilks, 1997, 2019) with 10,000 replicates. Based on objective criteria, we choose block lengths of $L_{FFDI} = 5$, $L_{CH} = 2$ and $L_{both} = 3$ for annual extreme occurrences of the FFDI, C-Haines, and both indices simultaneously, respectively. For a single test, we use a significance level of $\alpha_0 = 0.05$. When applying multiple tests simultaneously (as when applying the Pettitt test to each grid box in Australia), we control the false discovery rate (FDR; Benjamini and Hochberg, 1995) as recommended by a number of studies (Paciorek et al., 2002; Ventura et al., 2004; Wilks, 2016; Ivanov et al., 2018b,a; Wilks, 2019). We set $\alpha_{FDR} = 0.1$, allowing, on average, for 10% of statistically significant results to be erroneous (i.e. the null hypotheses are true). Applying a block bootstrap and controlling the FDR can have a substantial impact on the number of statistically significant results for our application. For a full technical description and a discussion of these results, see Appendix A.

We define a step change in some process as a statistically significant result from applying the Pettitt test according to the described procedure.

2.3. Atmospheric circulation diagnostics

As diagnostics of the atmospheric circulation we use five variables from JRA55: mean sea-level pressure (MSLP), geopotential height at 500 hPa, temperature at 850 hPa, meridional wind at 850 hPa and vertically-integrated water vapour transport (IVT; see Appendix B). We generate daily anomalies of these variables with respect to the daily averages computed over the period 1958–2019. This is achieved by computing individual day-of-year averages over all years, and then subtracting these from the original data. Composite (time-mean) fields of the anomalies are calculated on extreme fire weather index days and on different time periods as required.

We also estimate the frequency of atmospheric blocking events in the Tasman Sea (at 160° E) using the Tibaldi–Molteni blocking index (Tibaldi and Molteni, 1990; Tibaldi et al., 1994). This index provides a binary indicator of whether a particular day at a given longitude is considered blocked, according to 500 hPa geopotential height gradient criteria (see Appendix B). We consider the annual frequency of occurrence of blocking days (as elsewhere, a year is considered as running from July through June), and the annual frequency of occurrence of the subset of blocking days for which the FFDI is extreme.

2.4. Fire and pyrocumulonimbus observations

We supplement our analysis of fire weather indices with observations of fire and pyrocumulonimbus. For fire, we use the satellite-observed burned area products FireCCI v5.1 from the European Space Agency Climate Change Initiative (Lizundia-Loiola et al., 2020), and C3S v1.0 from the Copernicus Climate Change Service. FireCCI provides burned area data from 2001 through 2019 and C3S extends the data through to April 2020. The data are the monthly burned area within 0.25° latitude by longitude grid boxes. As with the fire weather indices, we consider annual data as running from July through June of the following calendar year. As such, we do not use the first six months of data in 2001, and the 2019 total only covers July 2019 through April 2020. We consider burned area over southeast Australia, as well as the subset of this region that is considered forested, according to FireCCI
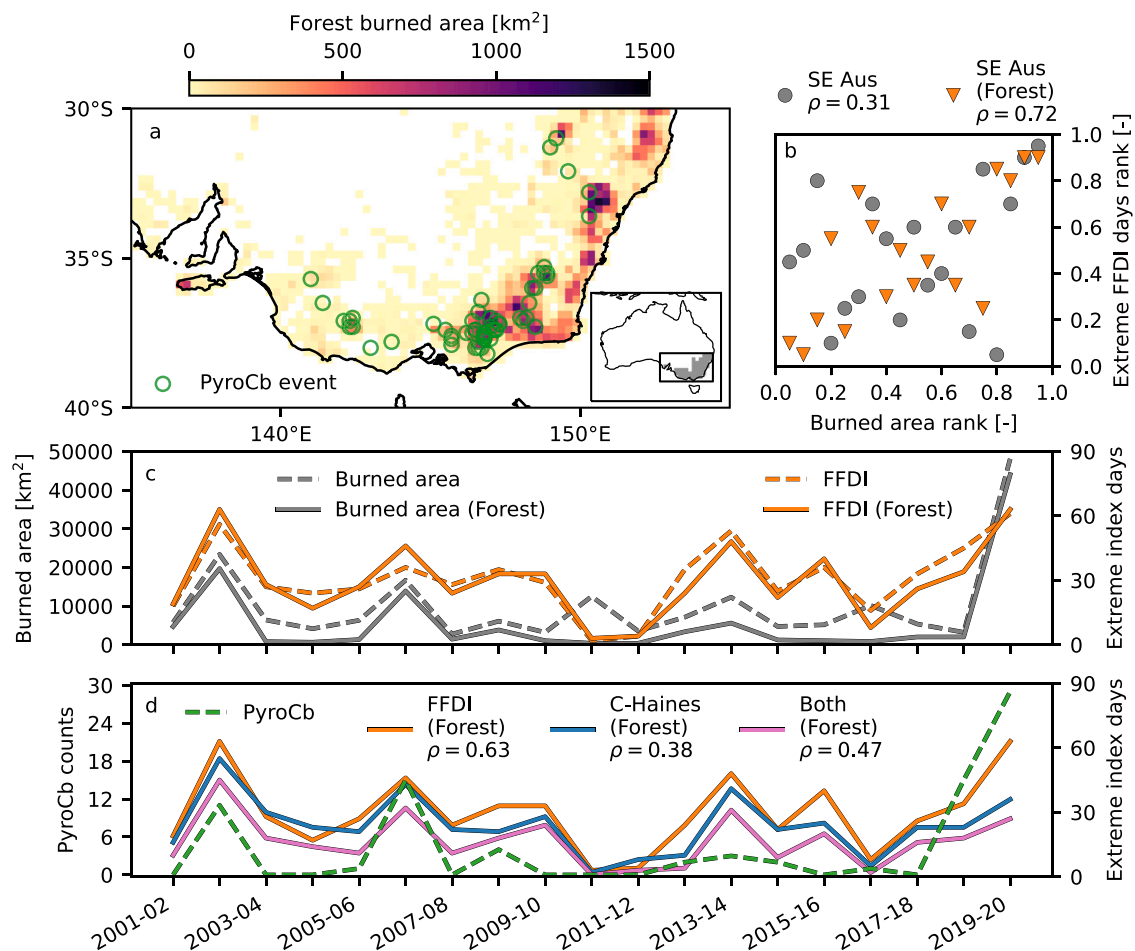
Fig. 1. Relationships between satellite-observed burned area, pyrocumulonimbus events and spatially-averaged fire weather indices. Panel a shows the total burned area for forest grid boxes in southeast Australia 2001 to 2019 (where the year spans July to June). White area is non-forested. Grey shading in the inset shows the forested cells on the JRA55 grid. Pyrocumulonimbus events up to April 2019 are represented by green circles (including four events prior to 2001). Panel b shows the relationship between burned area and the annual number of extreme FFDI days for southeast Australia (grey circles) and for forested regions of southeast Australia (orange triangles). The data are expressed in their rank order and scaled to lie between zero and one. The Spearman rank correlation coefficient, ρ, is shown in the legend. Panel c shows the time series of burned area (grey lines; left axis) and annual counts of extreme FFDI days (orange lines; right axis) for southeast Australia (solid) and forested regions of southeast Australia (dashed). Panel d shows the time series for the number of observed pyrocumulonimbus events per year (green dashed line; left axis) and the number of annual extreme days of the FFDI, C-Haines and both indices together (orange, blue and pink lines, respectively; right axis) for forested regions. The pyrocumulonimbus total for 2019 is from Abram et al. (2021). The legend shows Spearman's ρ between the annual number of pyrocumulonimbus and each of the fire weather indices. In all cases, an extreme value of a fire weather index is defined as when it is above the 95th percentile. (For interpretation of the references to colour in this figure legend, the reader is referred to the web version of this article.)

land cover categories 50–90. When comparing forest burned area data with fire weather indices, it is desirable to consider only those JRA55 grid boxes that align with the finer-resolution forest grid boxes. As such, if a JRA55 grid box encompasses at least 10 forest grid boxes from the burned area data (40% of the area of a JRA55 grid box), we consider it as forested (see Fig. S.3 in the supplementary material).

We also utilise pyrocumulonimbus observations obtained from the April 2019 version of the Australian pyrocumulonimbus register (Table S3 in the supporting information of Di Virgilio et al., 2019). This contains 82 identified pyrocumulonimbus events (Fig. S.4 in the supplementary material). The earliest occurred on Ash Wednesday (16 February 1983; Mills, 2005b), but there are only four events before 2000, reflecting the increased focus on monitoring in recent decades (Sharples et al., 2016). Although we do not have data for the timing and spatial location of pyrocumulonimbus occurrences since April 2019, we supplement annual totals with the 2019 data from Abram et al. (2021), who showed that there were 29 events in southeast Australia. That total includes a remarkable 18 occurrences between 29 December 2019 and 4 January 2020 alone (Kablick et al., 2020).

3. Results

3.1. Fire weather, burned area and pyrocumulonimbus

We begin with an exploratory analysis of the relationship between fire weather indices, burned area data and pyrocumulonimbus events. In southeast Australia (excluding Tasmania), large areas of forest were burned between 2001 and 2019, particularly along the southeast coast (Fig. 1a). The 2019 fire season was by far the most destructive in this period, with ~45,000 square kilometres burned (solid grey line in Fig. 1c), accounting for the vast majority of total area burned (i.e. forested or otherwise; dashed grey line in Fig. 1c).

There is evidence that the FFDI has a stronger relationship with burned area for forested regions than when the land cover type is not accounted for. This is shown by the relationship between annual counts of extreme FFDI days and burned area data: the dependence between the two variables is stronger for forested regions than otherwise, with a correspondingly larger Spearman's correlation coefficient ($\rho = 0.72$ compared to $\rho = 0.31$; Fig. 1b). The unprecedented burned area in 2019 is matched by the high number of extreme FFDI days, which is record-breaking for the entire region and record-equalling with 2002 for forested regions. This relationship between the FFDI and burned

area is in agreement with Abram et al. (2021) and Canadell et al. (2021), who used different FFDI statistics (September–February mean FFDI, and number of days with FFDI above 25 or 50, respectively).

Observed pyrocumulonimbus in southeast Australia have occurred predominantly over forests (Fig. 1a), potentially due, in part, to the high intensity at which eucalypt forest can burn (Bradstock, 2010). There are years for which spikes in the number of observed pyrocumulonimbus are matched by higher counts of extreme FFDI, C-Haines and co-occurring days (2002, 2006 and 2019; Fig. 1d). Correlation scores between annual pyrocumulonimbus and extreme fire weather index counts are modest. Interestingly, the correlation is strongest for extreme FFDI days ($\rho = 0.63$), rather than for extreme C-Haines days ($\rho = 0.38$) or days in which both indices are extreme ($\rho = 0.47$). Abram et al. (2021) showed that the warm-season (September to February) FFDI is a useful indicator of pyrocumulonimbus occurrence, with a record-breaking FFDI in 2019 matched by record-breaking number of pyrocumulonimbus events. This suggests that the FFDI is also a useful predictor of pyrocumulonimbus, at least for extreme values of the index.

As only 19 data points (years) are available, these results are likely to be associated with large uncertainty. Nevertheless, they accord with findings from Abram et al. (2021), who showed that increases in the FFDI are associated with greater fire intensity, providing further evidence of a dependence between fire weather indices and both fires and pyrocumulonimbus.

3.2. Changes in extreme fire weather occurrence

In this section we analyse the seasonality and changing behaviour of forest area-averaged fire weather indices. Fig. 2 shows the days on which the fire weather indices are extreme between July 1958 and June 2020, with summary plots for annual and seasonality statistics.

In 2019 there were 63 extreme FFDI days, the joint highest on record with 2002 (Fig. 2a). Both of these years were notable for severe fire events. The 2019 Black Summer fires caused unprecedented burning of forests in southeast Australia (Boer et al., 2020), with severe impacts on the environment and communities (Filkov et al., 2020). December 2019 featured a particularly high number of extreme FFDI days, including the maximum forest area-averaged FFDI on record (30 December 2019, FFDI = 39). January 2003 also featured a high number of extreme FFDI days. This corresponds to fires that burned large areas of Australia's alpine regions, with significant impacts to Canberra on 18 January (Bureau of Meteorology, 2003; Mills, 2005a). Fig. 2a also highlights three other significant fire events that correspond to extreme FFDI days: Ash Wednesday in 1983 (Mills, 2005b), the 2006 alpine fires (McCarthy et al., 2012) and Black Saturday 2009 (Cruz et al., 2012; Engel et al., 2013; Dowdy et al., 2017).

It is clear that extreme FFDI days have increased in frequency with time (Fig. 2a). This increase may represent a sudden shift in the mean, as it meets our criteria for a step change (a statistically significant result from the Pettitt test; $p < 0.01$). This step change occurred in 1997, marking an average increase of 14 extreme days per year from the earlier (1958–1997) to the later (1998–2019) period. In the later period, extreme FFDI days occur more frequently as consecutive, multi-day events, with events of at least three days in length over twice as likely. The potential impact of this is exacerbated by the fact that such events tend to be of a greater severity (i.e. a higher percentile): 43% of 99th percentile FFDI days occur as part of three-day (or longer) events, compared to 15% of 95th percentile FFDI days.

Extreme FFDI days have a clear seasonality, occurring primarily from October through March, peaking in December/January and with limited occurrence in the cold season. However, extreme FFDI days are now more likely both earlier and later in the fire season, as shown by the predominantly dark blue bars prior to October and after March in the bottom bar plot of Fig. 2a. From 1998, extreme FFDI days have

increased by a factor of nearly two and a half (one and a half) during July through October (March through June), compared to 1958–1997.

Extreme C-Haines days occur an average of eight days per year more frequently since 1998 (total bar height in the right-hand plot of Fig. 2b; $p = 0.07$). In comparison with the FFDI, extreme C-Haines days are spread more evenly throughout the year (bottom bar plot). As with the FFDI, from 1998 onwards extreme C-Haines days are more likely (roughly twice as likely) from July through October, in agreement with Dowdy and Pepler (2018). However, in contrast with that study, from the 1958–1997 and 1998–2019 periods we find a decrease in extreme C-Haines occurrences for March through June, by a factor of 1.2. Not all recorded pyrocumulonimbus events coincided with an extreme C-Haines day (grey circles in Fig. 2b). This is probably in part because pyrocumulonimbus are localised events in comparison to the region over which the C-Haines is averaged here.

The C-Haines index estimates the atmospheric stability and humidity to indicate the potential for pyrocumulonimbus events. Yet there are other factors that contribute to the formation of pyrocumulonimbus. In particular, a prerequisite for their development is fire, the weather-related risk of which can be measured with the FFDI. It is therefore instructive to consider those days which feature weather conditions most conducive to fire and the atmospheric instability characteristics of pyrocumulonimbus i.e. the subset of days that are extreme for both C-Haines and the FFDI (orange and brown bars in Fig. 2b). Indeed, of those days for which pyrocumulonimbus and extreme C-Haines coincide, the FFDI is also extreme, as shown by the grey circles over orange/brown bars in Fig. 2b (rather than over blue bars). This association of pyrocumulonimbus events with high values of the FFDI and C-Haines is in agreement with other studies (Mills and McCaw, 2010; Di Virgilio et al., 2019).

As with extreme C-Haines alone, for the 1998–2019 period there is an ~8 day increase in the average annual frequency of concurrent extreme FFDI and C-Haines compared to the 1958–1997 period. As with the FFDI, this change is abrupt enough to meet the criteria for a step change ($p = 0.02$). Again comparing the same periods, average annual occurrences of concurrent extreme days have increased for July through October by roughly a factor of 2.7, with no change for March through June. Increases in the co-occurrence of extreme days of these two indices are consistent with those from Dowdy and Pepler (2018). We also find that the number of three-day (or longer) events of concurrently extreme FFDI and C-Haines has increased almost seven-fold, from an average of one third to two such events per year.

To provide detail of the spatial variability of changes in fire weather, we now consider extreme FFDI and C-Haines days at the grid box scale. Within the southeast Australia region (Fig. 1a), each grid cell experiences up to 24 more extreme FFDI days per year after the year of a potential step change (Fig. 3d), consistent with long-term changes shown by Dowdy (2018). These changes satisfy the step change criteria, occurring between 1995 and 2000 for a number of grid boxes on the south coast of southeast mainland Australia (the most common step change year is 1997; dark orange in Fig. 3a). A greater number of grid boxes located more inland and to the northwest also show evidence of a step change between 2000 and 2005 (light blue).

The frequency of extreme C-Haines days has increased in recent decades throughout southeast Australia. As with the regional average, there is no statistical support for a step change (Fig. 3b, e). For this index, accounting for multiple testing has a large impact on the number of statistically significant results. Despite the very small p values in this region, controlling the false discovery rate yields a low number of significant results (Fig. A.1).

Co-occurring extreme FFDI and C-Haines days have increased in frequency by up to 10 days per year in southeast Australia since the late 1990s (Fig. 3c and f). Along the south coast of this region, these shifts constitute a step change, and correspond both spatially and in the timing of the shifts to the FFDI alone.
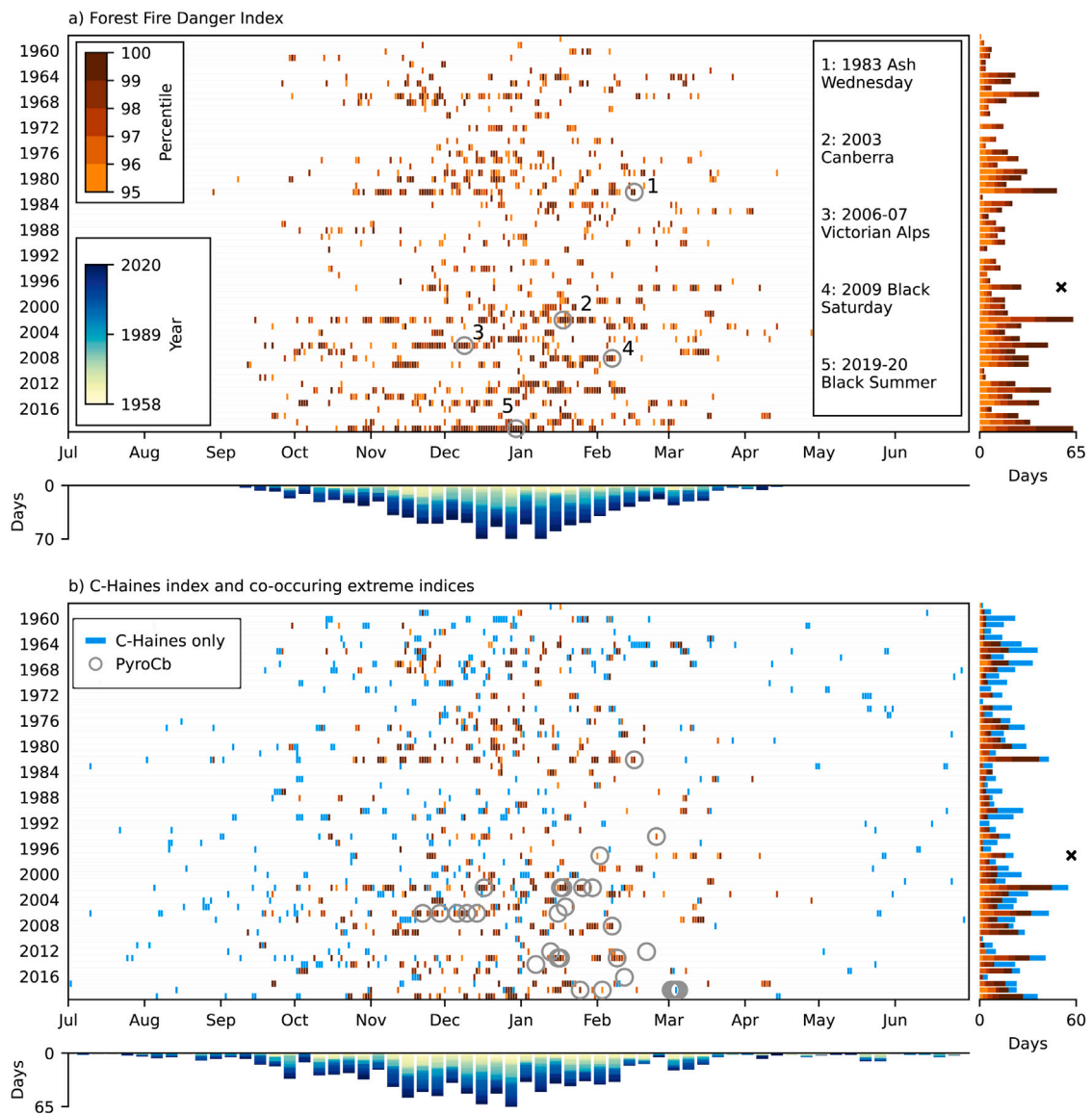
Fig. 2. Extreme FFDI (a) and C-Haines (b) occurrences July 1958 to June 2020 for the spatial average of the forested regions in southeast Australia. The extreme days are represented by bars and are coloured according to their percentile. In panel b, days that are extreme for C-Haines alone are coloured blue. Co-occurring extreme C-Haines and FFDI days are coloured orange and brown according to the C-Haines percentile, using the same colour scale as shown in panel a. Notable fire events are identified in panel a with grey circles. For the long-running events of 2006-07 and 2019-20, the day of highest FFDI is circled as a representative date. Grey circles in panel b represent observed pyrocumulonimbus events between 1983 and April 2019. The yearly totals of extreme days are shown in the bar plots on the right, also coloured by percentile. The cross in panel a indicates the year in which a step change (a statistically significant Pettitt test result) in extreme FFDI days is identified. The cross in panel b indicates a step change in co-occurring extreme FFDI and C-Haines. No step change was identified for extreme C-Haines alone. The seasonality is expressed as the total number of extreme days in six day intervals in the bar plots below. These counts are coloured according to the year in which they occurred. The legends do not obscure any data except for that in panel b, which obscures two extreme C-Haines days, in 1961 and 1970. (For interpretation of the references to colour in this figure legend, the reader is referred to the web version of this article.)

Parts of northern Australia have seen a decrease in the number of extreme FFDI days per year (Fig. 3a and d), in agreement with other studies (Dowdy, 2018; Dowdy and Pepler, 2018). There is also evidence of downward step changes of up to 24 (15) extreme C-Haines (co-occurring C-Haines and FFDI) days per year that occurred in the early to mid 1970s (Fig. 3b, c, e, f). We do not further analyse this result as pyrocumulonimbus events almost exclusively occur in southern Australia (only two of the pyrocumulonimbus events in the dataset used here occurred north of 25° S).

3.3. Changes in fire weather index components

To explore the potential causes of changes in extreme fire weather occurrence, we analyse changes in the FFDI and C-Haines component

(input) variables. As with the fire weather indices, we define an extreme value of an index component variable as when it is above the 95th percentile (or below the 5th percentile for relative humidity). We focus on a small domain within southeast Australia indicated by the rectangle in Fig. 3. This study region, which we call southwest Victoria, represents a compromise of step changes that occurred at similar times for the FFDI and for the combined FFDI/C-Haines. It is also a region that has suffered from forest burning and pyrocumulonimbus events (Fig. 1a).

The southwest Victoria annual extreme FFDI has increased over time, undergoing an upward step change in 1996 by ~40% (by a value of 6.5; $p < 0.001$; Fig. 4a), one year earlier than the step change in the number of extreme FFDI days per year (Fig. 2a). The probability density functions (PDFs) of daily FFDI values for the 1958–1997 and
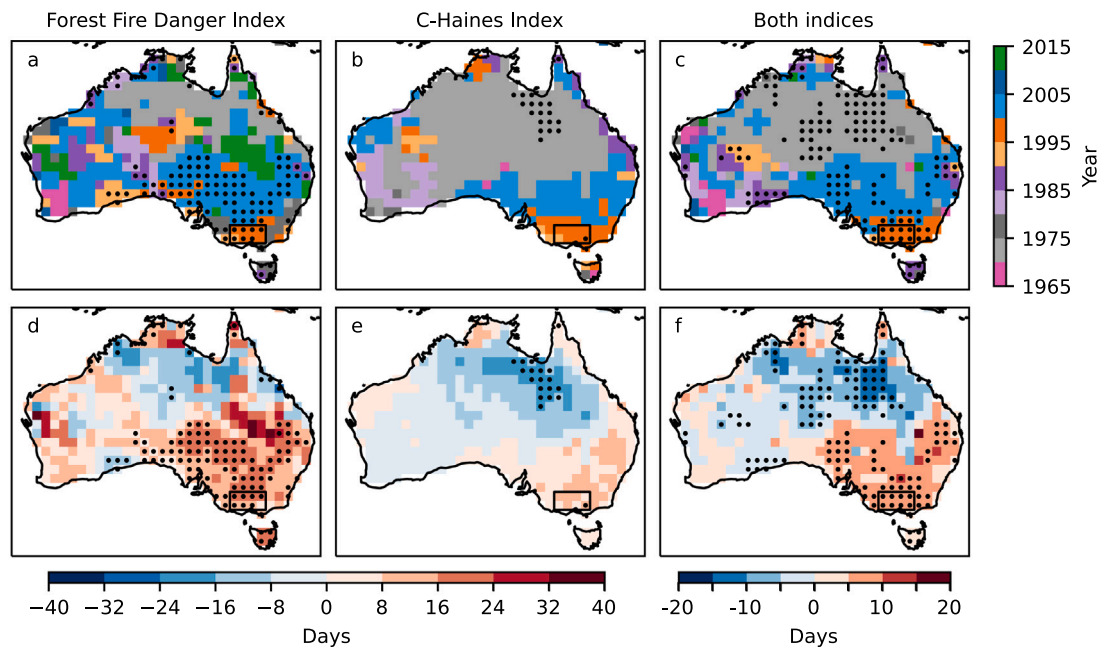
Fig. 3. Change in annual occurrence of extreme FFDI (left column), C-Haines (middle column) and co-occurring extreme indices (right column). The top row shows the year (τ) of a potential step change (i.e. the year corresponding to the Pettitt test statistic K_T). Stippling indicates statistical significance, meeting our criteria for identifying a step change. The bottom row shows the change in the average annual occurrence of extreme index days from prior to after the (potential) shift. The rectangle in southeast mainland Australia indicates our study region of southwest Victoria used in Fig. 4.

1998–2019 periods show a shift towards higher FFDI in the later period (Fig. 4b), both on all days (blue lines) and on extreme FFDI days only (red and orange lines). Furthermore, we obtain statistically significant results from applying two-sample Kolomogorov–Smirnov and Anderson–Darling tests (α = 0.05 Kolmogorov, 1933; Anderson, 1962) comparing the data between the two periods. This suggests that the samples of the two periods are drawn from different distributions.

Step changes concomitant with that of the FFDI are also found for the extreme values of the index's component variables. In the same year, annual extreme temperature increased by 1.6 °C (p = 0.003) and annual extreme relative humidity decreased by 5.8% (p < 0.001; Fig. 4g, j). Annual extreme wind speed also underwent a step change of 2.0 km/h, although earlier than the other variables, in 1985 (p = 0.001; Fig. 4m). Annual extreme values of the drought factor, however, display little discernible long-term change (Fig. 4d), corresponding to limited evidence for southern Australia precipitation trends found by other studies (Murphy and Timbal, 2008; Dey et al., 2019).

Comparing the PDFs of the FFDI component variables reveals their relative importance in determining the severity of the FFDI, with temperature and relative humidity the most important variables. When the FFDI is extreme (i.e. above the 95th percentile), the temperature and relative humidity values almost exclusively fall in the appropriate tails (upper tail for temperature, lower tail for relative humidity; Fig. 4h, i, k, l). The drought factor and wind speed are typically higher than normal during extreme FFDI days, but can take a wider range of values than temperature or relative humidity (Fig. 4e, f, n, o).

There are shifts in the PDFs of some FFDI components between 1958–1997 and 1998–2019, computed over all days and over extreme days (middle column of Fig. 4). In particular, relative humidity has decreased on all days (blue lines) and on extreme FFDI days (orange and red lines). Expressing the PDFs of the extreme FFDI days as percentiles of the climatology highlights a change in the far tail of the relative humidity PDF, with a greater number of days in the lowest few percentiles in the later period (Fig. 4l). Wind speed increased in 1998–2019 compared to 1958–1997, to a greater degree for all days than for extreme FFDI days (Fig. 4n). While temperature has increased over all days (blue lines of Fig. 4h), it has decreased slightly

on extreme FFDI days (red and orange lines of Fig. 4h, i). As with the FFDI, Kolomogorov–Smirnov and Anderson–Darling tests yield statistically significant results for all component variables, indicating that the population distributions for the two periods are not the same.

In the previous section we showed that changes in the number of extreme C-Haines days are of lower magnitude than the FFDI. We therefore briefly describe changes in the C-Haines component variables, with the relevant figure in the supplementary material. Three variables comprise the C-Haines: temperature at 850 hPa (T_{850}), temperature at 700 hPa (T_{700}) and dew point depression at 850 hPa (DD_{850}). However, the C-Haines estimates the vertical atmospheric stability by subtracting T_{700} from T_{850} (Section 2). We therefore consider the two component variables of the C-Haines as the stability component (T_{850} minus T_{700}) and the humidity component (DD_{850}).

Changes in the annual number of extreme C-Haines days do not constitute a step change as defined here (Fig. 2b). However, we do identify a step change in the annual 95th percentile C-Haines in southwest Victoria (in 1999, p = 0.009; Fig. S.5 in the supplementary material). This change is small in magnitude (an increase of 0.6), and there is little change in the PDFs before and from 1998 (Fig. S.5b). Coincident with 2 m temperature, there is an upward step change in both T_{700} and T_{850}. However, changes in these variables cancel in such a way as to yield a gradual decrease in the stability component over time (Fig. S.5d, g, j). For an extreme value of C-Haines, both the stability and humidity components are generally in the upper tail of their climatological distributions (Fig. S.5f, o). There is a suggestion that the humidity component (i.e. DD_{850}) has increased gradually over time, with a small-magnitude step change in 1990 (p = 0.03; Fig. S.5 m). Note that an increase in dew point depression over time indicates a trend towards more dry, unstable atmospheric conditions. This finding is consistent with Dowdy et al. (2019), who found that the humidity component is the primary driver of projected increases in southern Australia extreme C-Haines days for 2060–79.

3.4. Changes in atmospheric circulation

We further explore possible drivers of changes in extreme fire weather occurrence by analysing changes in the associated atmospheric
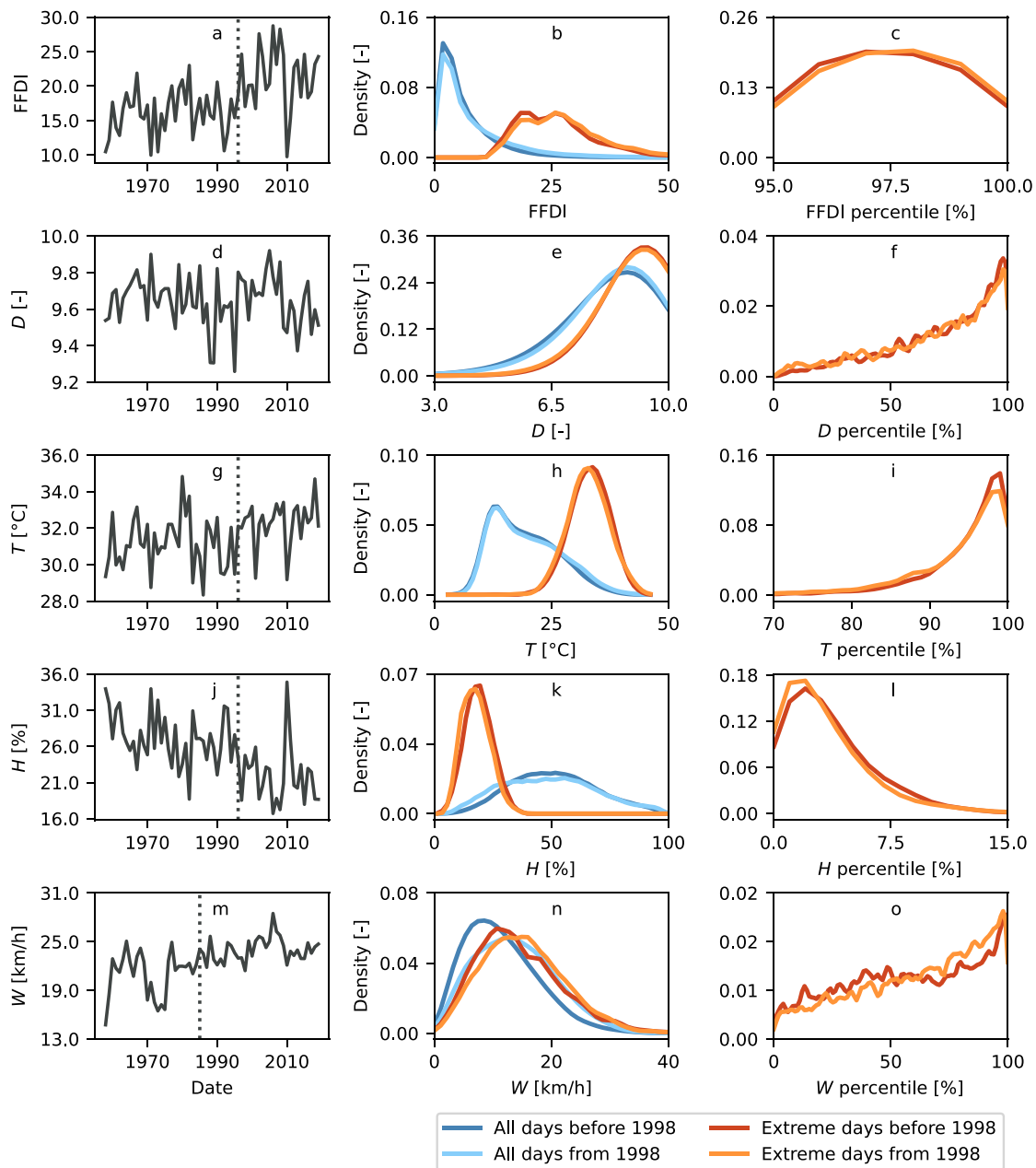
Fig. 4. Changes in FFDI (a–c) and its component variables: the drought factor (*D*; d–f), 2 m temperature (*T*; g–i), 2 m relative humidity (*H*; j–l) and 10 m wind speed (*W*; m–o) in the southwest Victoria study region. The left column is the spatially-averaged, annual 95th percentile of each variable (5th percentile for relative humidity). Dotted vertical lines indicate the detection of a step change. The middle column shows the climatological (all days) probability density function (PDF) of all grid boxes in the study region (i.e. not spatially averaged), split for the two periods 1958–1997 (dark blue) and 1998–2019 (light blue). Also shown are the PDFs for each variable on extreme FFDI days only (days when the FFDI is above the 95th percentile climatology), again split into 1958–1997 (red) and 1998–2019 (orange). The right column also shows the PDFs for the extreme FFDI days, but expressed as percentiles of the climatology (i.e. the two blue PDFs in the middle column combined). In most cases the *x*-axes of the middle and right columns are clipped to emphasise the majority of the data. (For interpretation of the references to colour in this figure legend, the reader is referred to the web version of this article.)

circulation. We use the step change identified for the grid box containing Melbourne as a means for splitting our data into two periods, before and from 1998.

The typical atmospheric set-up for fires in southeast Australia involves the approach and the passage of a cold front embedded in a trough (Voice and Gauntlett, 1984; Mills, 2005a,b; Cruz et al., 2012; Engel et al., 2013; Fiddes et al., 2016). Strong northwesterly winds ahead of the trough advect hot, dry air from the centre of the continent. Once the front has passed, the wind generally swings round to southwesterly, broadening the fire front.

The atmospheric circulation associated with fire weather has been studied primarily for individual events (Voice and Gauntlett, 1984; Mills, 2005a,b; Cruz et al., 2012; Engel et al., 2013; Fiddes et al., 2016),

while another study analysed composites over 43 extreme summer cold front events (Reeder et al., 2015). We explicitly consider atmospheric diagnostics associated with 1,139 extreme FFDI days (i.e. those above the 95th percentile), finding that the synoptic structure is very similar to that found for summer cold fronts (Reeder et al., 2015), despite the large differences in sample size. We present results for extreme FFDI days only, as those for extreme C-Haines days and co-occurring extreme index days are very similar.

The described synoptic set-up is evident for extreme FFDI days near Melbourne (the grid box centred at 145° E, 37.5° S; Fig. 5). From roughly one week prior to extreme FFDI days, a large-scale wave train propagates eastwards along the storm track from the southern Atlantic to Australian longitudes. Anomalous cyclonic and anticyclonic nodes
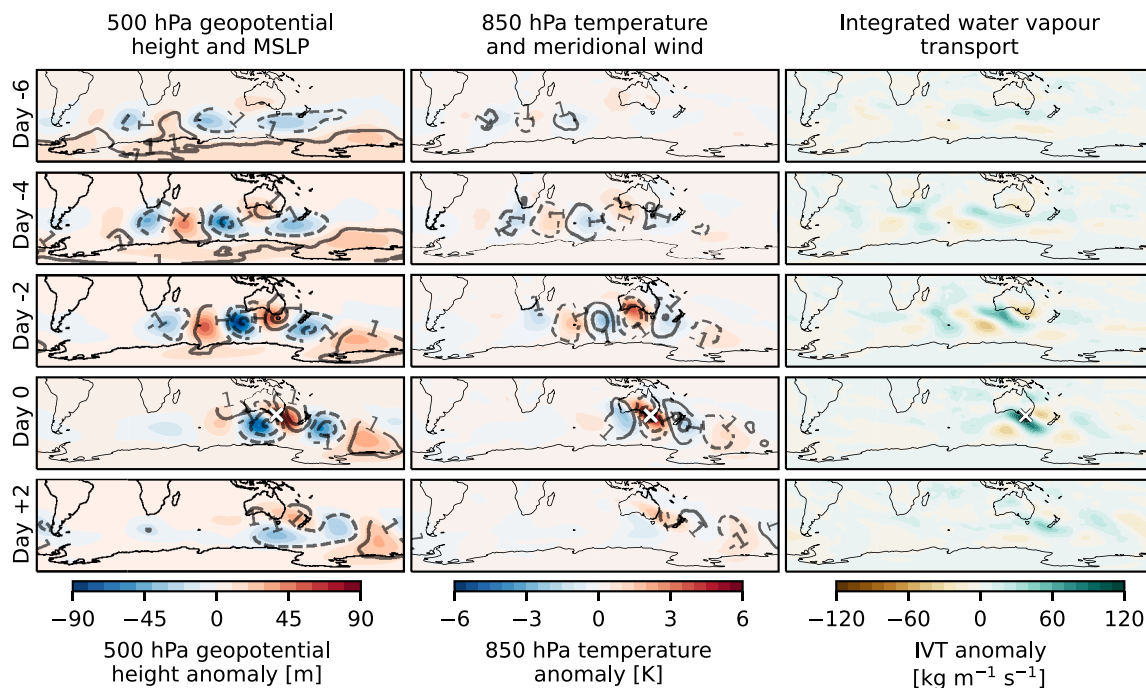
Fig. 5. Atmospheric diagnostics during the lifecycle of Melbourne (140° E, 37.5° S; marked with a white cross in the 'Day 0' row) extreme FFDI days. The left column shows the geopotential height at 500 hPa (shading) and mean sea-level pressure (MSLP; contours, labelled at −1 and 1 hPa, and spaced in intervals of 2 hPa). The middle column shows the temperature (shading) and meridional wind (contours, labelled at −1 and 1 m/s, and spaced in intervals of 2 m/s) at 850 hPa. The third column shows the vertically-integrated water vapour transport (IVT). The 'Day 0' row shows composites on extreme FFDI days. The rows above show composites for six, four and two days prior; the row below shows composites for two days after.

at the surface and in the mid-troposphere increase in intensity as the event nears (left column). The propagation of these features along ∼45° S implies that extreme FFDI days are set up by storm track dynamics rather than the subtropical ridge, which is located at lower latitudes (Pittock, 1973; Larsen and Nicholls, 2009). This assessment is bolstered by the presence of strong pressure anomalies throughout the column of atmosphere (i.e. at the surface and at 500 hPa). The deep structure implies the high pressure anomaly in the Tasman Sea on the day of the event is an anticyclone rather than a weaker ridge, which is typically associated with the surface only (Pittock, 1973; Larsen and Nicholls, 2009).

Corresponding with the atmospheric circulation dipole over southeast Australia, anomalous 850 hPa meridional winds and temperatures are evident, increasing in magnitude in the lead-up to the event (middle column). Changes to climatological atmospheric water vapour are also clear. In particular, two days prior to the event there is a clear reduction in IVT over southeast Australia (right column).

On the day of the event ('Day 0' in Fig. 5), a surface trough extends into southern Australia, with associated cyclonic anomalies in the mid-troposphere located slightly upstream (left column). The strong pressure gradient over Melbourne results in northerly wind anomalies, which in turn drive anomalously high temperatures (middle column). The cold front that follows such events is clearly marked by a band of anomalously high IVT southwest of Melbourne (right column).

Changes in the atmospheric circulation from 1998 are consistent with the increased annual occurrence of extreme FFDI days. Since then, the 500 hPa geopotential heights have increased over southern Australia and in the mid-latitudinal Pacific Ocean, and decreased southeast of New Zealand (Fig. 6c), indicating a poleward contraction of the storm track in this region (Kushner et al., 2001; Yin, 2005; Harvey et al., 2012; Yang et al., 2020). This is broadly consistent with a trend towards the positive phase of the Southern Annular Mode (SAM), one of the drivers of Australian climate variability, identified by observational, reanalysis and climate change studies (Thompson and Solomon, 2002; Fyfe, 2003; Swart et al., 2015). In addition, the temperature at 850 hPa

has increased by up to 0.5 K for much of the southern hemisphere, and up to 1 K over Australia (Fig. 6d).

The changes associated with extreme FFDI days have similar signatures as those over all days, but with higher magnitude anomalies, especially south of Australia (Fig. 6e, f). In particular, the blocking node of the wave train over the Tasman Sea (Fig. 6a) has amplified on extreme FFDI days from 1998 (Fig. 6e). This intensification is associated with increased 850 hPa temperatures of up to 1.5 K (Fig. 6f).

We use the Tibaldi–Molteni blocking index calculated at 160° E to assess the extent to which the amplified node of Tasman Sea anticyclonic anomalies can be ascribed to changes in blocking frequency. The frequency of blocked days per year has decreased since the 1980s (Fig. 7), in agreement with findings from other studies (Wiedenmann et al., 2002; O'Kane et al., 2013, 2016). Despite this, the proportion of extreme FFDI days near Melbourne that are considered blocked has increased, with most years since the mid-1990s featuring a number of blocked, extreme FFDI days. From 1998, the average annual frequency of such days is 3.8%, compared to 1.6% for the preceding 22 years.

4. Discussion and conclusions

Attempts to model potential changes in fire weather as a step change (as presented here) or a linear trend (Clarke et al., 2013; Jolly et al., 2015; Harris and Lucas, 2019; Canadell et al., 2021) are not expected to fully encapsulate the dynamics involved. Nevertheless, regardless of the most suitable model for these changes, the evidence here and from other studies strongly indicates that, in the past two decades, extreme fire weather in southeast Australia has become more severe and more frequent, and occurs over a longer season.

Our analysis shows that extreme fire weather occurrence in southeast Australia has increased over recent decades. In parts of southeast Australia, these increases appear to have occurred rapidly, as evidenced by statistical support for a step change in the number of extreme FFDI days per year. This step change occurred in 1997 for southwest Victoria and in the early 2000s for more northern and western regions. There
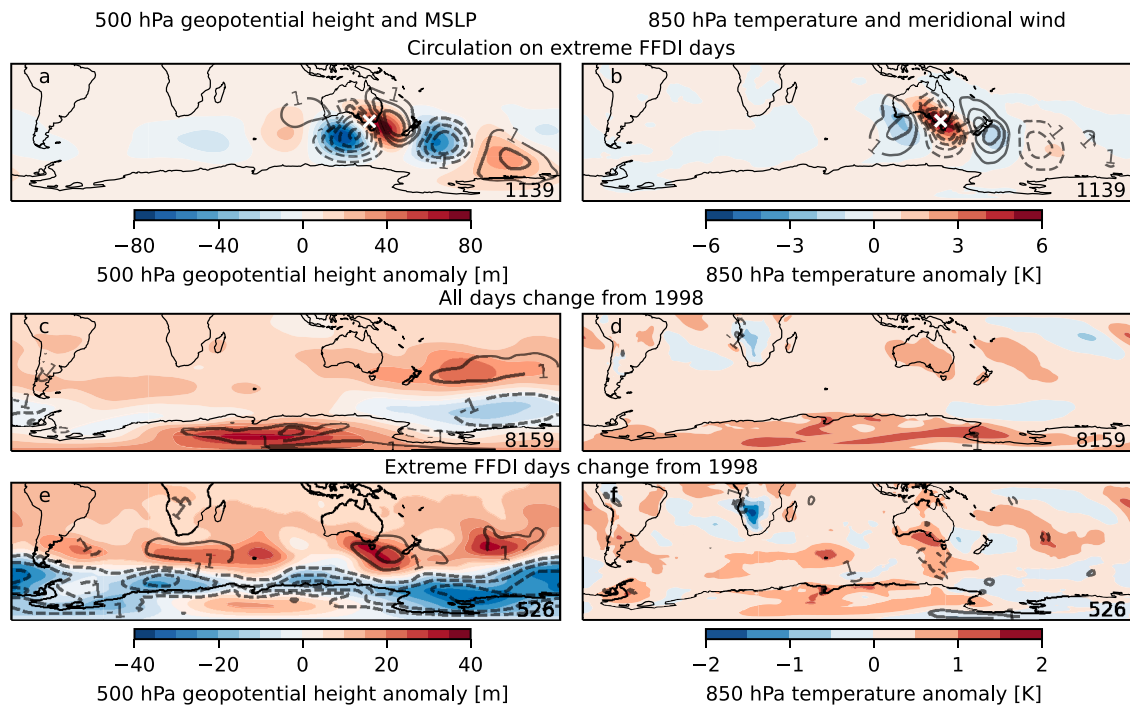
Fig. 6. Atmospheric diagnostics on Melbourne (140° E, 37.5° S; marked with a white cross) extreme FFDI days and changes over time. The left column shows the geopotential height at 500 hPa (shading) and mean sea-level pressure (MSLP; contours, labelled at −1 and 1 hPa, and spaced in intervals of 1 hPa). The right column shows the temperature (shading) and meridional wind (contours, labelled at −1 and 1 m/s, and spaced in intervals of 1 m/s) at 850 hPa. Panels a and b show composites associated with extreme FFDI days 1958–2019. Panels c and d show the mean field for all days 1998–2019 minus the mean field for all days 1976–1997. Panels e and f show the composites for the 526 extreme FFDI days from July 1998 minus the composites for the most recent 526 extreme days prior to July 1998 (the earliest such day occurred in 1965). Sample sizes (in days) are shown in the bottom right of each panel.
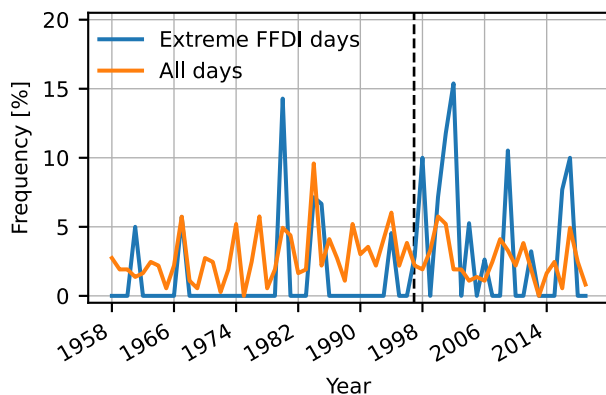
Fig. 7. Annual Tibaldi–Molteni blocking index frequency [%] at 160° E, calculated with respect to all days (orange) and to extreme FFDI days in Melbourne (140° E, 37.5° S; blue). The dashed vertical line at June 1998 marks the step change in annual counts of extreme FFDI days. (For interpretation of the references to colour in this figure legend, the reader is referred to the web version of this article.)

is evidence from observational data suggesting that fire activity in southeast Australia increased in the early 2000s (Fairman et al., 2016; Sharples et al., 2016; Lindenmayer and Taylor, 2020; Abram et al., 2021; Canadell et al., 2021), corresponding with the sharp rise in the number of extreme FFDI days found here. That these changes in fire and in the FFDI are related is supported by relatively strong correlations between the two variables and by evidence from other studies suggesting the index is an important predictor of fire severity and intensity (Tolhurst and McCarthy, 2016; Abram et al., 2021; Canadell et al., 2021).

The changes in extreme FFDI days in the smaller region of southwest Victoria are concomitant with changes in extreme annual values of

2 m temperature and relative humidity. Since 1998, extreme FFDI days are characterised by higher wind speeds and lower relative humidity. However, temperature on extreme FFDI days is slightly lower, despite rising overall.

One can only go so far in attributing changes in observed pyrocumulonimbus to changes in the two fire weather indices used here. This is due to the short observational record, and to the importance of other processes involved in pyrocumulonimbus development, such as the fire behaviour, fuel condition and type of terrain (e.g. McRae et al., 2015; Tory and Thurston, 2015; Di Virgilio et al., 2019). Nevertheless, we find evidence that one aspect indicating greater potential for pyrocumulonimbus formation, the atmospheric instability as measured by extreme values of the C-Haines index, is more prevalent since 1998 compared to the two decades prior across southeast Australia.

We posit that a contributing factor to potential increases in pyrocumulonimbus events is an increase in extreme FFDI days (insofar as the short observational record allows). We show that in forested regions, the number of extreme FFDI days bears a stronger relationship to pyrocumulonimbus occurrence than the C-Haines does, although the small sample size means these results may be subject to large uncertainty and the differences statistically insignificant. Nevertheless, our findings accord with those of other studies that found evidence of a relationship between the FFDI and pyrocumulonimbus (Di Virgilio et al., 2019; Abram et al., 2021). A consequence of the increased prevalence of extreme FFDI days is an increased number of days in which the index co-occurs with an extreme C-Haines. This increased co-occurrence suggests that atmospheric and surface weather conditions are now more conducive to the formation of pyrocumulonimbus. As we do not find evidence that the structure of C-Haines has changed, we may partly explain the observed increase in pyrocumulonimbus without recourse to any change in the stability properties of the atmosphere, but just from the increase in extreme fire weather days.

The fire weather atmospheric circulation is associated with a large-scale wave train across Indian, Australian and Pacific longitudes. The

wave train contains nodes corresponding to a block in the Tasman Sea and an approaching trough, which together create a strong pressure gradient, northerly flow and high temperatures characteristic of extreme fire weather days. This wave train propagates eastwards towards Australia across the oceanic basins from the south Atlantic over a period of about a week, and bears a strong resemblance to the dynamics associated with a small sample of extreme summertime cold fronts (Reeder et al., 2015).

Consistent with findings from other studies, the circulation changes from 1998 onwards suggest a poleward contraction of the storm track (Kushner et al., 2001; Thompson and Solomon, 2002; Fyfe, 2003; Yin, 2005; Harvey et al., 2012; Swart et al., 2015; Yang et al., 2020). Such changes have been linked to reduced winter precipitation in southeast Australia (Timbal and Drosdowsky, 2013; Delworth and Zeng, 2014; Pepler, 2020). This may result in priming the landscape for the following fire season.

On extreme FFDI days, the shift in the storm track is accompanied by enhanced Tasman Sea anticyclonic anomalies, resulting in an increased pressure gradient and hence stronger northerlies and higher tropospheric temperatures. Moreover, this enhanced anticyclonic node may reflect an increase in the frequency of blocking on extreme FFDI days, despite the decrease in the overall frequency of blocking days. Increases in 500 hPa geopotential heights and blocking events in this region are in turn consistent with lower relative humidity and higher wind speeds near the surface driving extreme FFDI days from 1998.

Warmer temperatures and reduced continental relative humidity are both signatures of climate change (Byrne and O'Gorman, 2018). Similarly, the southerly shift of the storm track in Australian longitudes is consistent with greenhouse forcing (Kushner et al., 2001; Thompson and Solomon, 2002; Fyfe, 2003; Yin, 2005; Harvey et al., 2012; Swart et al., 2015; Yang et al., 2020). Understanding the variability of fire weather will require more work on these, and other, processes, but the long-term trends will likely reflect ongoing warming and continental drying induced by greenhouse climate change.

Code availability and software

The code is available on request from the corresponding author. The code was written in Python 3 with the following packages: Cartopy (Met Office, 2015), Dask (Dask Development Team, 2016), Matplotlib (Hunter, 2007), pandas (McKinney, 2010), NumPy (van der Walt et al., 2011) and xarray (Hoyer and Hamman, 2017).

CRediT authorship contribution statement

Doug Richardson: Conceptualization, Methodology, Software, Formal analysis, Investigation, Writing – original draft, Writing – review & editing, Visualization. **Amanda S. Black:** Writing – review & editing. **Didier P. Monselesan:** Data curation, Writing – review & editing. **James S. Risbey:** Conceptualization, Writing – review & editing. **Dougal T. Squire:** Data curation, Writing – review & editing. **Carly R. Tozer:** Writing – review & editing. **Josep G. Canadell:** Writing – review & editing.

Declaration of competing interest

The authors declare that they have no known competing financial interests or personal relationships that could have appeared to influence the work reported in this paper.

Data availability

The data used for the fire weather indices and atmospheric circulation diagnostics are from the Japanese Meteorological Agency 55-year reanalysis product (Agency, 2013), publicly available at https://rda.ucar.edu/datasets/ds628.0/. The European Space Agency FireCCI v5.1 and Copernicus Climate Change Service C3S v1.0 burned area data is available at https://cds.climate.copernicus.eu/cdsapp#!/dataset/satellite-fire-burned-area. Pyrocumulonimbus observations are taken from Table S3 in the supporting information of Di Virgilio et al. (2019), and the 2019-20 total is from Abram et al. (2021).

Acknowledgements

Appendix A. Pettitt test statistical significance

We use the Pettitt test (Pettitt, 1979) to assess the presence of abrupt changes in time series of annual counts of extreme fire weather index days. As with many statistical tests, an assumption of the Pettitt test is that the data should be serially independent. Applying the test to autocorrelated data typically results in an over-rejection of the null hypothesis i.e. the identification of an abrupt change when no such change is actually present (Busuioc and von Storch, 1996; Serinaldi and Kilsby, 2016). A straightforward method to try and account for autocorrelation is to use the block bootstrap (Kunsch, 1989; Lahiri, 2003; Wilks, 1997, 2019), which randomly resamples consecutive data values in 'blocks' of length L. To determine L, we assume that the data follow a first-order autoregressive (AR(1)) process and use the formula given by Wilks (1997):

$$L = (n - L + 1)^{(2/3)(1-n'/n)},\tag{A.1}$$

where n' is the effective sample size given by

$$n' \approx n\frac{1 - \rho_1}{1 + \rho_1},\tag{A.2}$$

and ρ_1 is the lag-1 autocorrelation coefficient. For simplicity, we use the spatial average of ρ_1 over mainland southeast Australia, as indicated by the inset of Fig. 1a. This yields block lengths of $L_{\text{FFDI}} = 5$, $L_{\text{CH}} = 2$ and $L_{\text{both}} = 3$ for annual extreme occurrences of the FFDI, C-Haines, and both indices simultaneously, respectively.

We generated 10,000 block-bootstrapped series of the same length as the original series ($n = 62$) and calculated the quantile q at which K_T (Eq. (4)) calculated from the original data lies in the bootstrapped sample. The p value is then $p = 1 - q$. For the evaluation of a single test, we choose $\alpha_0 = 0.05$ and determine the result as statistically significant when $p < \alpha_0$.

For part of our analysis, we apply the Pettitt test to multiple, spatially correlated, grid boxes simultaneously. As with autocorrelation, this can result in an over-rejection of the null hypothesis if not properly accounted for. We therefore control the false discovery rate (FDR; Benjamini and Hochberg, 1995) as recommended by a number of studies (Paciorek et al., 2002; Ventura et al., 2004; Wilks, 2016; Ivanov et al., 2018b,a). The FDR approach ranks the p values arising from the N tests in ascending order, $p_{(1)}, \ldots, p_{(N)}$. A test is considered significant if $p < p_{\text{FDR}}$, where

$$p_{\text{FDR}} = \max_{j=1,\ldots,N}\left\{ p_{(j)} : p_{(j)} \leq \frac{j}{N}\alpha_{\text{FDR}} \right\}.\tag{A.3}$$

Following Wilks (2016), we set $\alpha_{\text{FDR}} = 2\alpha_0 = 0.1$, allowing, on average, for 10% of statistically significant results ('discoveries') to be
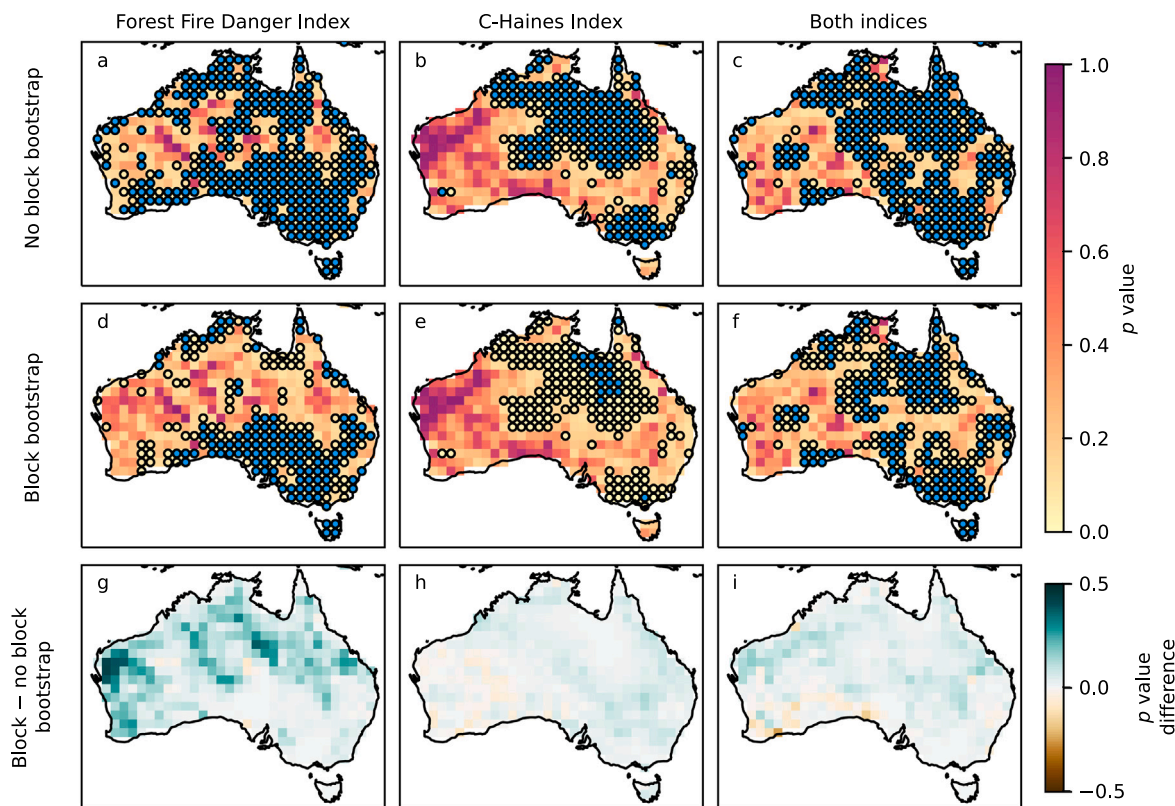
Fig. A.1. Resultant p values from applying the Pettitt test to annual counts of extreme FFDI days (left column), C-Haines days (middle column) and days for which both indices are extreme (right column). In the top row, 'standard' i.e. non-block bootstrapping is used. In the middle row, a block bootstrap is used with block sizes of $L_{FFDI} = 5$, $L_{CH} = 2$ and $L_{both} = 3$. Open circle stippling indicates significant results defined as when $p < \alpha_0$. Blue stippling indicates significant results defined when $p < p_{FDR}$. The significance levels are set as $\alpha_0 = \alpha_{FDR} = 0.1$, ensuring that the statistically significant results arising from applying the FDR correction are a subset of those with no FDR correction. The difference in p values arising from applying a block bootstrap versus no block bootstrap are shown in the bottom row. (For interpretation of the references to colour in this figure legend, the reader is referred to the web version of this article.)

erroneous (i.e. the null hypotheses are true). However, from Eq. (A.3) we see that if $\alpha_{FDR} = \alpha_0$, then statistically significant results from using $p < p_{FDR}$ will be a subset of those from using $p < \alpha_0$. To illustrate this, for the following discussion we set $\alpha_0 = \alpha_{FDR} = 0.1$.

In Fig. A.1, we show the effects of applying a block bootstrap and the FDR approach on resulting statistical significance. When neither are applied, and $p < \alpha_0$ is used to assign significance, there are a large number of discoveries for each fire weather index (all stippling in top row). When applying either FDR (filled stippling in top row) or the block bootstrap (all stippling in second row), the latter has a greater effect on reducing the number of discoveries. Finally, controlling the FDR and using a block bootstrap (filled stippling in second row) further reduces the number of statistically significant results, particularly for the C-Haines index. Note that the block bootstrap alters the p values, whereas FDR does not. In general, applying a block bootstrap results in larger p values, particularly for the FFDI in northern and western Australia (bottom row).

Appendix B. Atmospheric circulation diagnostics

Vertically-integrated water vapour transport (IVT) is calculated using JRA55 daily data as

$$\text{IVT} = \sqrt{\left(\frac{1}{g}\int_{\text{sfc}}^{300\text{hPa}} qu\,dp\right)^2 + \left(\frac{1}{g}\int_{\text{sfc}}^{300\text{hPa}} qv\,dp\right)^2}, \quad (B.1)$$

where u and v are the zonal and meridional components of wind speed, respectively, q is specific humidity and g is the acceleration due to gravity (Benedict et al., 2019; Black et al., 2021).

The Tibaldi–Molteni blocking index (Tibaldi and Molteni, 1990; Tibaldi et al., 1994) is calculated as follows. We apply a five-day running mean to 500 hPa geopotential height fields at 160° E from the Japanese 55-year reanalysis product (JRA55; Japan Meteorological Agency, 2013). Following Tibaldi et al. (1994), the following geopotential height gradients are evaluated:

$$\text{GHGS} = \frac{z(\phi_S) - z(\phi_O)}{\phi_S - \phi_O} \quad (B.2)$$

$$\text{GHGN} = \frac{z(\phi_O) - z(\phi_N)}{\phi_O - \phi_N}, \quad (B.3)$$

where $\phi_N = 35°S + \Delta$, $\phi_O = 50°S + \Delta$, $\phi_S = 65°S + \Delta$, and $\Delta = -5°, 0°, 5°$. A given day at a particular longitude is considered blocked if, for any Δ, the following conditions are satisfied:

$$\text{GHGS} < \frac{-10 \text{ m}}{(\text{degree of latitude})} \quad (B.4)$$

$$\text{GHGN} > 0. \quad (B.5)$$

Appendix C. Supplementary data

Supplementary material related to this article can be found online at https://doi.org/10.1016/j.wace.2021.100397.

References

Abram, N.J., Hargreaves, J.A., Wright, N.M., Thirumalai, K., Ummenhofer, C.C., England, M.H., 2020. Palaeoclimate perspectives on the Indian Ocean Dipole. Quat. Sci. Rev. (ISSN: 0277-3791) 237, 106302. http://dx.doi.org/10.1016/j.quascirev.2020.106302.

Abram, N.J., Henley, B.J., Sen Gupta, A., Lippmann, T.J.R., Clarke, H., Dowdy, A.J., Sharples, J.J., Nolan, R.H., Zhang, T., Wooster, M.J., Wurtzel, J.B., Meissner, K.J., Pitman, A.J., Ukkola, A.M., Murphy, B.P., Tapper, N.J., Boer, M.M., 2021. Connections of climate change and variability to large and extreme forest fires in southeast Australia. Commun. Earth Environ. (ISSN: 2662-4435) 2 (1), 1–17. http://dx.doi.org/10.1038/s43247-020-00065-8, Number: 1 Publisher: Nature Publishing Group.

Anderson, T.W., 1962. On the distribution of the two-sample cramer-von mises criterion. Ann. Math. Stat. (ISSN: 0003-4851) 33 (3), 1148–1159. http://dx.doi.org/10.1214/aoms/1177704477.

Arblaster, J.M., Meehl, G.A., 2006. Contributions of external forcings to southern annular mode trends. J. Clim. 19 (12), 2896–2905. http://dx.doi.org/10.1175/JCLI3774.1, (ISSN: 0894-8755, 1520-0442). Publisher: American Meteorological Society Section: Journal of Climate.

Bárdossy, A., Caspary, H.J., 1990. Detection of climate change in Europe by analyzing European atmospheric circulation patterns from 1881 to 1989. Theor. Appl. Climatol. (ISSN: 1434-4483) 42 (3), 155–167. http://dx.doi.org/10.1007/BF00866871.

Benedict, J.J., Clement, A.C., Medeiros, B., 2019. Atmospheric blocking and other large-scale precursor patterns of landfalling atmospheric rivers in the north Pacific: A CESM2 study. J. Geophys. Res.: Atmos. (ISSN: 2169-8996) 124 (21), 11330–11353. http://dx.doi.org/10.1029/2019JD030790, _eprint: https://agupubs.onlinelibrary.wiley.com/doi/pdf/10.1029/2019JD030790.

Benjamini, Y., Hochberg, Y., 1995. Controlling the false discovery rate: A practical and powerful approach to multiple testing. J. R. Stat. Soc. Ser. B Stat. Methodol. (ISSN: 0035-9246) 57 (1), 289–300. http://dx.doi.org/10.1111/j.2517-6161.1995.tb02031.x, Publisher: John Wiley & Sons, Ltd.

Black, A.S., Risbey, J.S., Chapman, C.C., Monselesan, D.P., II, T.S.M., Pook, M.J., Richardson, D., Sloyan, B.M., Squire, D.T., Tozer, C.R., 2021. Australian northwest cloudbands and their relationship to atmospheric rivers and precipitation. Mon. Weather Rev. 149 (4), 1125–1139. http://dx.doi.org/10.1175/MWR-D-20-0308.1, Place: Boston MA, USA Publisher: American Meteorological Society.

Blanchi, R., Leonard, J., Haynes, K., Opie, K., James, M., Oliveira, F.D.d., 2014. Environmental circumstances surrounding bushfire fatalities in Australia 1901–2011. Environ. Sci. Policy (ISSN: 1462-9011) 37, 192–203. http://dx.doi.org/10.1016/j.envsci.2013.09.013.

Blanchi, R., Lucas, C., Leonard, J., Finkele, K., 2010. Meteorological conditions and wildfire-related houseloss in Australia. Int. J. Wildland Fire (ISSN: 1448-5516) 19 (7), 914–926. http://dx.doi.org/10.1071/WF08175, Publisher: CSIRO PUBLISHING.

Boer, M.M., Resco de Dios, V., Bradstock, R.A., 2020. Unprecedented burn area of Australian mega forest fires. Nature Clim. Change (ISSN: 1758-6798) 10 (3), 171–172. http://dx.doi.org/10.1038/s41558-020-0716-1, Number: 3 Publisher: Nature Publishing Group.

Bradstock, R.A., 2010. A biogeographic model of fire regimes in Australia: current and future implications. Global Ecol. Biogeogr. (ISSN: 1466-822X) 19 (2), 145–158. http://dx.doi.org/10.1111/j.1466-8238.2009.00512.x.

Bradstock, R., Penman, T., Boer, M., Price, O., Clarke, H., 2014. Divergent responses of fire to recent warming and drying across south-eastern Australia. Global Change Biol. (ISSN: 1365-2486) 20 (5), 1412–1428. http://dx.doi.org/10.1111/gcb.12449, _eprint: https://onlinelibrary.wiley.com/doi/pdf/10.1111/gcb.12449.

Bureau of Meteorology, 2003. Meteorological aspects of the Eastern Victorian Fires January-March 2003. Tech. Rep., Bureau of Meteorology, URL: http://www.bom.gov.au/weather-services/fire-weather-centre/weather-patterns/past-bushfires/Eastern_Victoria_Fires_Jan_Mar_2003.pdf.

Busuioc, A., von Storch, H., 1996. Changes in the winter precipitation in Romania and its relation to the large-scale circulation. Tellus A (ISSN: 1600-0870) 48 (4), 538–552. http://dx.doi.org/10.1034/j.1600-0870.1996.t01-3-00004.x, _eprint: https://onlinelibrary.wiley.com/doi/pdf/10.1034/j.1600-0870.1996.t01-3-00004.x.

Byrne, M.P., O'Gorman, P.A., 2018. Trends in continental temperature and humidity directly linked to ocean warming. Proc. Natl. Acad. Sci. 115 (19), 4863. http://dx.doi.org/10.1073/pnas.1722312115.

Cai, W., Cowan, T., Raupach, M., 2009a. Positive Indian ocean dipole events precondition southeast Australia bushfires. Geophys. Res. Lett. (ISSN: 0094-8276) 36 (19), http://dx.doi.org/10.1029/2009GL039902, Publisher: John Wiley & Sons, Ltd.

Cai, W., Cowan, T., Sullivan, A., 2009b. Recent unprecedented skewness towards positive Indian Ocean Dipole occurrences and its impact on Australian rainfall. Geophys. Res. Lett. (ISSN: 0094-8276) 36 (11), http://dx.doi.org/10.1029/2009GL037604, Publisher: John Wiley & Sons, Ltd.

Cai, W., Zheng, X.-T., Weller, E., Collins, M., Cowan, T., Lengaigne, M., Yu, W., Yamagata, T., 2013. Projected response of the Indian Ocean Dipole to greenhouse warming. Nat. Geosci. (ISSN: 1752-0908) 6 (12), 999–1007. http://dx.doi.org/10.1038/ngeo2009.

Canadell, J.G., Meyer, M.C.P., Cook, G., Dowdy, A.J., Briggs, P.R., Knauer, J., Pepler, A.S., Haverd, V., 2021. Multi-decadal increase of forest burned area in Australia is linked to climate change. Nature Commun. 12, 6921. http://dx.doi.org/10.1038/s41467-021-27225-4.

Clarke, H., Lucas, C., Smith, P., 2013. Changes in Australian fire weather between 1973 and 2010. Int. J. Climatol. (ISSN: 0899-8418) 33 (4), 931–944. http://dx.doi.org/10.1002/joc.3480.

Cruz, M., Sullivan, A., Gould, J., Sims, N., Bannister, A., Hollis, J., Hurley, R., 2012. Anatomy of a catastrophic wildfire: The Black Saturday Kilmore East fire in Victoria, Australia. Forest Ecol. Manag. (ISSN: 0378-1127) 284, 269–285. http://dx.doi.org/10.1016/j.foreco.2012.02.035.

Dask Development Team, 2016. Dask: Library for dynamic task scheduling. URL: https://dask.org (visited on 03/03/2020).

Delworth, T.L., Zeng, F., 2014. Regional rainfall decline in Australia attributed to anthropogenic greenhouse gases and ozone levels. Nat. Geosci. (ISSN: 1752-0908) 7 (8), 583–587. http://dx.doi.org/10.1038/ngeo2201, Number: 8 Publisher: Nature Publishing Group.

Dey, R., Lewis, S.C., Arblaster, J.M., Abram, N.J., 2019. A review of past and projected changes in Australia's rainfall. WIREs Clim. Chang. (ISSN: 1757-7780) 10 (3), e577. http://dx.doi.org/10.1002/wcc.577, Publisher: John Wiley & Sons, Ltd.

Di Virgilio, G., Evans, J.P., Blake, S.A.P., Armstrong, M., Dowdy, A.J., Sharples, J., McRae, R., 2019. Climate change increases the potential for extreme wildfires. Geophys. Res. Lett. (ISSN: 0094-8276) 46 (14), 8517–8526. http://dx.doi.org/10.1029/2019GL083699.

Dowdy, A.J., 2018. Climatological variability of fire weather in Australia. J. Appl. Meteorol. Climatol. (ISSN: 1558-8424) 57 (2), 221–234. http://dx.doi.org/10.1175/JAMC-D-17-0167.1.

Dowdy, A.J., Fromm, M.D., McCarthy, N., 2017. Pyrocumulonimbus lightning and fire ignition on Black Saturday in southeast Australia. J. Geophys. Res.: Atmos. (ISSN: 2169-897X) 122 (14), 7342–7354. http://dx.doi.org/10.1002/2017JD026577.

Dowdy, A.J., Pepler, A., 2018. Pyroconvection risk in Australia: Climatological changes in atmospheric stability and surface fire weather conditions. Geophys. Res. Lett. (ISSN: 0094-8276) 45 (4), 2005–2013. http://dx.doi.org/10.1002/2017GL076654.

Dowdy, A.J., Ye, H., Pepler, A., Thatcher, M., Osbrough, S.L., Evans, J.P., Virgilio, G.D., McCarthy, N., 2019. Future changes in extreme weather and pyroconvection risk factors for Australian wildfires. Sci. Rep. (ISSN: 2045-2322) 9 (1), 1–11. http://dx.doi.org/10.1038/s41598-019-46362-x.

Engel, C.B., Lane, T.P., Reeder, M.J., Rezny, M., 2013. The meteorology of Black Saturday. Q. J. R. Meteorol. Soc. (ISSN: 0035-9009) 139 (672), 585–599. http://dx.doi.org/10.1002/qj.1986.

Fairman, T.A., Bennett, L.T., Nitschke, C.R., 2019. Short-interval wildfires increase likelihood of resprouting failure in fire-tolerant trees. J. Environ. Manag. (ISSN: 0301-4797) 231, 59–65. http://dx.doi.org/10.1016/j.jenvman.2018.10.021.

Fairman, T.A., Nitschke, C.R., Bennett, L.T., 2016. Too much, too soon? A review of the effects of increasing wildfire frequency on tree mortality and regeneration in temperate eucalypt forests. Int. J. Wildland Fire 25 (8), 831–848.

Ferguson, C.R., Villarini, G., 2012. Detecting inhomogeneities in the Twentieth Century Reanalysis over the central United States. J. Geophys. Res.: Atmos. (ISSN: 2156-2202) 117 (D5), http://dx.doi.org/10.1029/2011JD016988, _eprint: https://agupubs.onlinelibrary.wiley.com/doi/pdf/10.1029/2011JD016988.

Fiddes, S.L., Pezza, A.B., Renwick, J., 2016. Significant extra-tropical anomalies in the lead up to the Black Saturday fires. Int. J. Climatol. (ISSN: 0899-8418) 36 (2), 1011–1018. http://dx.doi.org/10.1002/joc.4387.

Filkov, A.I., Ngo, T., Matthews, S., Telfer, S., Penman, T.D., 2020. Impact of Australia's catastrophic 2019/20 bushfire season on communities and environment. Retrospective analysis and current trends. J. Saf. Sci. Resil. (ISSN: 2666-4496) 1 (1), 44–56. http://dx.doi.org/10.1016/j.jnlssr.2020.06.009.

Finkele, K., Mills, G.A., Beard, G., Jones, D.A., 2006. National gridded drought factors and comparison of two soil moisture deficit formulations used in prediction of Forest Fire Danger Index in Australia. Aust. Meteorol. Mag. 55 (3), 183–197, URL: https://citeseerx.ist.psu.edu/viewdoc/download?doi=10.1.1.222.8769&rep=rep1&type=pdf.

Fromm, M., McRae, R.H.D., Sharples, J.J., Kablick, III, G.P., 2012. Pyrocumulonimbus pair in Wollemi and Blue Mountains National Parks, 22 November 2006. Aust. Meteorol. Oceanogr. J. (ISSN: 1836-716X) 62 (3), 117–126.

Fyfe, J.C., 2003. Extratropical southern hemisphere cyclones: Harbingers of climate change? J. Clim. (ISSN: 0894-8755) 16 (17), 2802–2805. http://dx.doi.org/10.1175/1520-0442(2003)016<2802:ESHCHO>2.0.CO;2, Publisher: American Meteorological Society.

Gill, A.M., Stephens, S.L., Cary, G.J., 2013. The worldwide "wildfire" problem. Ecol. Appl. (ISSN: 1051-0761) 23 (2), 438–454. http://dx.doi.org/10.1890/10-2213.1, Publisher: John Wiley & Sons, Ltd.

Haines, D.A., 1988. A lower atmospheric severity index for wildland fires. Natl. Weather Digest 13 (3), 23–27.

Harada, Y., Kamahori, H., Kobayashi, C., Endo, H., Kobayashi, S., Ota, Y., Onoda, H., Onogi, K., Miyaoka, K., Takahashi, K., 2016. The JRA-55 reanalysis: Representation of atmospheric circulation and climate variability. J. Meteorol. Soc. Jpn. Ser. II 94 (3), 269–302. http://dx.doi.org/10.2151/jmsj.2016-015, (ISSN: 0026-1165, 2186-9057).

Harris, S., Anderson, W., Kilinc, M., Fogarty, L., 2012. The relationship between fire behaviour measures and community loss: an exploratory analysis for developing a bushfire severity scale. Nat. Hazards (ISSN: 1573-0840) 63 (2), 391–415. http://dx.doi.org/10.1007/s11069-012-0156-y.

Harris, S., Lucas, C., 2019. Understanding the variability of Australian fire weather between 1973 and 2017. PLoS One 14 (9), e0222328. http://dx.doi.org/10.1371/journal.pone.0222328, Publisher: Public Library of Science.

Harvey, B.J., Shaffrey, L.C., Woollings, T.J., Zappa, G., Hodges, K.I., 2012. How large are projected 21st century storm track changes? Geophys. Res. Lett. (ISSN: 0094-8276) 39 (18), http://dx.doi.org/10.1029/2012GL052873, Publisher: John Wiley & Sons, Ltd.

Hoyer, S., Hamman, J., 2017. xarray: N-D labeled arrays and datasets in Python. J. Open Res. Softw. 5 (1), 10. http://dx.doi.org/10.5334/jors.148.

Hunter, J.D., 2007. Matplotlib: A 2D graphics environment. Comput. Sci. Eng. (ISSN: 1558-366X) 9 (3), 90–95. http://dx.doi.org/10.1109/MCSE.2007.55.

Ivanov, M., Warrach-Sagi, K., Wulfmeyer, V., 2018a. Field significance of performance measures in the context of regional climate model evaluation. Part 1: temperature. Theor. Appl. Climatol. (ISSN: 1434-4483) 132 (1), 219–237. http://dx.doi.org/10.1007/s00704-017-2100-2.

Ivanov, M., Warrach-Sagi, K., Wulfmeyer, V., 2018b. Field significance of performance measures in the context of regional climate model evaluation. Part 2: precipitation. Theor. Appl. Climatol. (ISSN: 1434-4483) 132 (1), 239–261. http://dx.doi.org/10.1007/s00704-017-2077-x.

Japan Meteorological Agency, 2013. JRA-55: Japanese 55-year reanalysis, daily 3-hourly and 6-hourly data. http://dx.doi.org/10.5065/D6HH6H41.

Jolly, W.M., Cochrane, M.A., Freeborn, P.H., Holden, Z.A., Brown, T.J., Williamson, G.J., Bowman, D.M.J.S., 2015. Climate-induced variations in global wildfire danger from 1979 to 2013. Nature Commun. (ISSN: 2041-1723) 6 (1), 7537. http://dx.doi.org/10.1038/ncomms8537.

Kablick, G.P., Allen, D.R., Fromm, M.D., Nedoluha, G.E., 2020. Australian PyroCb smoke generates synoptic-scale stratospheric anticyclones. Geophys. Res. Lett. (ISSN: 1944-8007) 47 (13), e2020GL088101. http://dx.doi.org/10.1029/2020GL088101, _eprint: https://agupubs.onlinelibrary.wiley.com/doi/pdf/10.1029/2020GL088101.

Kobayashi, S., Ota, Y., Harada, Y., Ebita, A., Moriya, M., Onoda, H., Onogi, K., Kamahori, H., Kobayashi, C., Endo, H., Miyaoka, K., Takahashi, K., 2015. The JRA-55 reanalysis: General specifications and basic characteristics. J. Meteorol. Soc. Jpn. Ser. II 93 (1), 5–48. http://dx.doi.org/10.2151/jmsj.2015-001, (ISSN: 0026-1165, 2186-9057).

Kolmogorov, A.N., 1933. Sulla Determinazione Empirica di una Legge di Distribuzione. G. Ist. Ital. Attuari 4, 83–91.

Kunsch, H.R., 1989. The jackknife and the bootstrap for general stationary observations. Ann. Statist. 17 (3), 1217–1241. http://dx.doi.org/10.1214/aos/1176347265, (ISSN: 0090-5364, 2168-8966). Publisher: Institute of Mathematical Statistics.

Kushner, P.J., Held, I.M., Delworth, T.L., 2001. Southern hemisphere atmospheric circulation response to global warming. J. Clim. (ISSN: 0894-8755) 14 (10), 2238–2249. http://dx.doi.org/10.1175/1520-0442(2001)014<0001:SHACRT>2.0.CO;2, Publisher: American Meteorological Society.

Lahiri, S.N., 2003. Bootstrap methods. In: Lahiri, S.N. (Ed.), Resampling Methods for Dependent Data. In: Springer Series in Statistics, Springer, New York, NY, ISBN: 978-1-4757-3803-2, pp. 17–43. http://dx.doi.org/10.1007/978-1-4757-3803-2_2.

Larsen, S.H., Nicholls, N., 2009. Southern Australian rainfall and the subtropical ridge: Variations, interrelationships, and trends. Geophys. Res. Lett. (ISSN: 1944-8007) 36 (8), http://dx.doi.org/10.1029/2009GL037786, _eprint: https://agupubs.onlinelibrary.wiley.com/doi/pdf/10.1029/2009GL037786.

Lindenmayer, D.B., Kooyman, R.M., Taylor, C., Ward, M., Watson, J.E.M., 2020. Recent Australian wildfires made worse by logging and associated forest management. Nat. Ecol. Evol. (ISSN: 2397-334X) http://dx.doi.org/10.1038/s41559-020-1195-5.

Lindenmayer, D.B., Taylor, C., 2020. New spatial analyses of Australian wildfires highlight the need for new fire, resource, and conservation policies. Proc. Natl. Acad. Sci. 202002269. http://dx.doi.org/10.1073/pnas.2002269117.

Lizundia-Loiola, J., Otón, G., Ramo, R., Chuvieco, E., 2020. A spatio-temporal active-fire clustering approach for global burned area mapping at 250 m from MODIS data. Remote Sens. Environ. (ISSN: 0034-4257) 236, 111493. http://dx.doi.org/10.1016/j.rse.2019.111493.

Luke, R.H., McArthur, A.G., 1978. Bush Fires in Australia. Australian Government Publishing Service, Canberra, ACT.

McCarthy, G., Plucinski, M.P., Gould, J., 2012. Analysis of the resourcing and containment of multiple remote fires: The Great Divide Complex of fires, Victoria, December 2006. Aust. For. (ISSN: 0004-9158) 75 (1), 54–63. http://dx.doi.org/10.1080/00049158.2012.10676385, Publisher: Taylor & Francis _eprint: https://doi.org/10.1080/00049158.2012.10676385.

McKinney, W., 2010. Data structures for statistical computing in python. In: van der Walt, S., Millman, J. (Eds.), Proceedings of the 9th Python in Science Conference. pp. 51–56, URL: https://conference.scipy.org/proceedings/scipy2010/mckinney.html.

McRae, R.H.D., Sharples, J.J., Fromm, M., 2015. Linking local wildfire dynamics to pyroCb development. Nat. Hazards Earth Syst. Sci. 15 (3), 417–428. http://dx.doi.org/10.5194/nhess-15-417-2015.

Met Office, 2015. Cartopy: a cartographic python library with a matplotlib interface. URL: http://scitools.org.uk/cartopy (visited on 03/03/2020).

Mills, G.A., 2005a. On the subsynoptic-scale meteorology of two extreme fire weather days during the Eastern Australian fires of January 2003. Aust. Meteorol. Mag. 54 (4), 265–290, URL: http://www.bom.gov.au/jshess/docs/2005/mills2_hres.pdf.

Mills, G.A., 2005b. A re-examination of the synoptic and mesoscale meteorology of Ash Wednesday 1983. Aust. Meteorol. Mag. 54 (1), 35–55, URL: http://www.bom.gov.au/jshess/docs/2005/mills1_hres.pdf.

Mills, G.A., McCaw, L., 2010. Atmospheric Stability Environments and Fire Weather in Australia - extending the Haines index. Tech. Rep. 20, URL: https://www.cawcr.gov.au/technical-reports/CTR_020.pdf.

Moritz, M.A., Batllori, E., Bradstock, R.A., Gill, A.M., Handmer, J., Hessburg, P.F., Leonard, J., McCaffrey, S., Odion, D.C., Schoennagel, T., Syphard, A.D., 2014. Learning to coexist with wildfire. Nature (ISSN: 1476-4687) 515 (7525), 58–66. http://dx.doi.org/10.1038/nature13946.

Murphy, B.P., Bradstock, R.A., Boer, M.M., Carter, J., Cary, G.J., Cochrane, M.A., Fensham, R.J., Russell-Smith, J., Williamson, G.J., Bowman, D.M.J.S., 2013. Fire regimes of Australia: a pyrogeographic model system. J. Biogeogr. (ISSN: 0305-0270) 40 (6), 1048–1058. http://dx.doi.org/10.1111/jbi.12065, Publisher: John Wiley & Sons, Ltd.

Murphy, B.F., Timbal, B., 2008. A review of recent climate variability and climate change in southeastern Australia. Int. J. Climatol. (ISSN: 0899-8418) 28 (7), 859–879. http://dx.doi.org/10.1002/joc.1627, Publisher: John Wiley & Sons, Ltd.

Noble, I.R., Gill, A.M., Bary, G.A.V., 1980. McArthur's fire-danger meters expressed as equations. Aust. J. Ecol. (ISSN: 0307-692X) 5 (2), 201–203. http://dx.doi.org/10.1111/j.1442-9993.1980.tb01243.x.

O'Kane, T.J., Risbey, J.S., Franzke, C., Horenko, I., Monselesan, D.P., 2013. Changes in the metastability of the midlatitude southern hemisphere circulation and the utility of nonstationary cluster analysis and split-flow blocking indices as diagnostic tools. J. Atmos. Sci. 70 (3), 824–842. http://dx.doi.org/10.1175/JAS-D-12-028.1, (ISSN: 0022-4928, 1520-0469). Publisher: American Meteorological Society Section: Journal of Atmospheric Sciences.

O'Kane, T.J., Risbey, J.S., Monselesan, D.P., Horenko, I., Franzke, C.L.E., 2016. On the dynamics of persistent states and their secular trends in the waveguides of the Southern Hemisphere troposphere. Clim. Dynam. (ISSN: 1432-0894) 46 (11), 3567–3597. http://dx.doi.org/10.1007/s00382-015-2786-8.

Paciorek, C.J., Risbey, J.S., Ventura, V., Rosen, R.D., 2002. Multiple indices of northern hemisphere cyclone activity, winters 1949–99. J. Clim. (ISSN: 0894-8755) 15 (13), 1573–1590. http://dx.doi.org/10.1175/1520-0442(2002)015<1573:MIONHC>2.0.CO;2, Publisher: American Meteorological Society.

Pepler, A., 2020. Record lack of cyclones in southern Australia during 2019. Geophys. Res. Lett. (ISSN: 1944-8007) 47 (13), e2020GL088488. http://dx.doi.org/10.1029/2020GL088488, _eprint: https://agupubs.onlinelibrary.wiley.com/doi/pdf/10.1029/2020GL088488.

Pettitt, A.N., 1979. A non-parametric approach to the change-point problem. J. R. Stat. Soc. Ser. C Appl. Stat. 28 (2), 126–135. http://dx.doi.org/10.2307/2346729, (ISSN: 00359254, 14679876). Publisher: [Wiley, Royal Statistical Society].

Pittock, A.B., 1973. Global meridional interactions in stratosphere and troposphere. Q. J. R. Meteorol. Soc. (ISSN: 1477-870X) 99 (421), 424–437. http://dx.doi.org/10.1002/qj.49709942103, _eprint: https://rmets.onlinelibrary.wiley.com/doi/pdf/10.1002/qj.49709942103.

Plucinski, M.P., Sullivan, A.L., McCaw, W.L., 2020. Comparing the performance of daily forest fire danger summary metrics for estimating fire activity in southern Australian forests. Int. J. Wildland Fire.

Readfearn, G., 2019. Scientists fear surge in supersized bushfires that create their own violent thunderstorms. Section: Environment. URL: http://www.theguardian.com/environment/2019/dec/20/scientists-fear-surge-in-supersized-bushfires-that-create-their-own-violent-thunderstorms (visited on 01/18/2021).

Reeder, M.J., Spengler, T., Musgrave, R., 2015. Rossby waves, extreme fronts, and wildfires in southeastern Australia. Geophys. Res. Lett. (ISSN: 0094-8276) 42 (6), 2015–2023. http://dx.doi.org/10.1002/2015GL063125.

Russell-Smith, J., Yates, C.P., Whitehead, P.J., Smith, R., Craig, R., Allan, G.E., Thackway, R., Frakes, I., Cridland, S., Meyer, M.C.P., Gill, A.M., 2007. Bushfires down under: patterns and implications of contemporary Australian landscape burning. Int. J. Wildland Fire 16 (4), 361–377.

Serinaldi, F., Kilsby, C.G., 2016. The importance of prewhitening in change point analysis under persistence. Stoch. Environ. Res. Risk Assess. (ISSN: 1436-3259) 30 (2), 763–777. http://dx.doi.org/10.1007/s00477-015-1041-5.

Sharples, J.J., Cary, G.J., Fox-Hughes, P., Mooney, S., Evans, J.P., Fletcher, M.-S., Fromm, M., Grierson, P.F., McRae, R., Baker, P., 2016. Natural hazards in Australia: extreme bushfire. Clim. Change (ISSN: 1573-1480) 139 (1), 85–99. http://dx.doi.org/10.1007/s10584-016-1811-1.

Sharples, J.J., Mills, G.A., McRae, R.H.D., Weber, R.O., 2010. Foehn-like winds and elevated fire danger conditions in southeastern Australia. J. Appl. Meteorol. Climatol. (ISSN: 1558-8424) 49 (6), 1067–1095. http://dx.doi.org/10.1175/2010JAMC2219.1.

Simmons, A., Hersbach, H., Munoz-Sabater, J., Nicolas, J., Vamborg, F., Berrisford, P., de Rosnay, P., Willett, K., Woollen, J., 2021. Low Frequency Variability and Trends in Surface Air Temperature and Humidity from ERA5 and Other Datasets. Tech. Rep. 881, European Centre for Medium-Range Weather Forecasts, European Centre for Medium-Range Weather Forecasts, Shinfield Park, Reading, Berkshire RG2 9AX, England, http://dx.doi.org/10.21957/ly5vbtbfd, Publisher: ECMWF.

Swart, N.C., Fyfe, J.C., Gillett, N., Marshall, G.J., 2015. Comparing trends in the southern annular mode and surface westerly jet. J. Clim. (ISSN: 0894-8755) 28 (22), 8840–8859. http://dx.doi.org/10.1175/JCLI-D-15-0334.1, Publisher: American Meteorological Society.

Thompson, D.W.J., Solomon, S., 2002. Interpretation of recent southern hemisphere climate change. Science 296 (5569), 895. http://dx.doi.org/10.1126/science.1069270.

Thompson, D.W.J., Solomon, S., Kushner, P.J., England, M.H., Grise, K.M., Karoly, D.J., 2011. Signatures of the Antarctic ozone hole in Southern Hemisphere surface climate change. Nat. Geosci. (ISSN: 1752-0908) 4 (11), 741–749. http://dx.doi.org/10.1038/ngeo1296, Bandiera_abtest: a Cg_type: Nature Research Journals Number: 11 Primary_atype: Reviews Publisher: Nature Publishing Group Subject_term: Atmospheric science;Climate change;Climate-change impacts Subject_term_id: atmospheric-science;climate-change;climate-change-impacts.

Tibaldi, S., Molteni, F., 1990. On the operational predictability of blocking. Tellus A (ISSN: 1600-0870) 42 (3), 343–365. http://dx.doi.org/10.1034/j.1600-0870.1990.t01-2-00003.x, _eprint: https://onlinelibrary.wiley.com/doi/pdf/10.1034/j.1600-0870.1990.t01-2-00003.x.

Tibaldi, S., Tosi, E., Navarra, A., Pedulli, L., 1994. Northern and southern hemisphere seasonal variability of blocking frequency and predictability. Mon. Weather Rev. 122 (9), 1971–2003. http://dx.doi.org/10.1175/1520-0493(1994)122<1971:NASHSV>2.0.CO;2, (ISSN: 1520-0493, 0027-0644). Publisher: American Meteorological Society Section: Monthly Weather Review.

Timbal, B., Drosdowsky, W., 2013. The relationship between the decline of Southeastern Australian rainfall and the strengthening of the subtropical ridge. Int. J. Climatol. (ISSN: 1097-0088) 33 (4), 1021–1034. http://dx.doi.org/10.1002/joc.3492, _eprint: https://rmets.onlinelibrary.wiley.com/doi/pdf/10.1002/joc.3492.

Tolhurst, K.G., McCarthy, G., 2016. Effect of prescribed burning on wildfire severity: a landscape-scale case study from the 2003 fires in Victoria. Aust. For. (ISSN: 0004-9158) 79 (1), 1–14. http://dx.doi.org/10.1080/00049158.2015.1127197, Publisher: Taylor & Francis _eprint: https://doi.org/10.1080/00049158.2015.1127197.

Tory, K.J., Thurston, W., 2015. Pyrocumulonimbus: A Literature Review. Tech. Rep., Bushfire and Natural Hazards CRC, Bushfire and Natural Hazards CRC, East Melbourne, VIC, Australia, URL: https://www.bnhcrc.com.au/publications/biblio/bnh-1882.

van der Walt, S., Colbert, S.C., Varoquaux, G., 2011. The NumPy array: A structure for efficient numerical computation. Comput. Sci. Eng. (ISSN: 1558-366X) 13 (2), 22–30. http://dx.doi.org/10.1109/MCSE.2011.37.

Ventura, V., Paciorek, C.J., Risbey, J.S., 2004. Controlling the proportion of falsely rejected hypotheses when conducting multiple tests with climatological data. J. Clim. (ISSN: 0894-8755) 17 (22), 4343–4356. http://dx.doi.org/10.1175/3199.1, Publisher: American Meteorological Society.

Villarini, G., Serinaldi, F., Smith, J.A., Krajewski, W.F., 2009. On the stationarity of annual flood peaks in the continental United States during the 20th century. Water Resour. Res. (ISSN: 1944-7973) 45 (8), http://dx.doi.org/10.1029/2008WR007645, _eprint: https://agupubs.onlinelibrary.wiley.com/doi/pdf/10.1029/2008WR007645.

Voice, M.E., Gauntlett, F.J., 1984. The 1983 Ash wednesday fires in Australia. Mon. Weather Rev. (ISSN: 0027-0644) 112 (3), 584–590. http://dx.doi.org/10.1175/1520-0493(1984)112<0584:TAWFIA>2.0.CO;2.

Ward, M., Tulloch, A.I.T., Radford, J.Q., Williams, B.A., Reside, A.E., Macdonald, S.L., Mayfield, H.J., Maron, M., Possingham, H.P., Vine, S.J., O'Connor, J.L., Massingham, E.J., Greenville, A.C., Woinarski, J.C.Z., Garnett, S.T., Lintermans, M., Scheele, B.C., Carwardine, J., Nimmo, D.G., Lindenmayer, D.B., Kooyman, R.M., Simmonds, J.S., Sonter, L.J., Watson, J.E.M., 2020. Impact of 2019–2020 megafires on Australian fauna habitat. Nat. Ecol. Evol. (ISSN: 2397-334X) 4 (10), 1321–1326. http://dx.doi.org/10.1038/s41559-020-1251-1, Number: 10 Publisher: Nature Publishing Group.

Wiedenmann, J.M., Lupo, A.R., Mokhov, I.I., Tikhonova, E.A., 2002. The climatology of blocking anticyclones for the northern and southern hemispheres: Block intensity as a diagnostic. J. Clim. 15 (23), 3459–3473. http://dx.doi.org/10.1175/1520-0442(2002)015<3459:TCOBAF>2.0.CO;2, (ISSN: 0894-8755, 1520-0442). Publisher: American Meteorological Society Section: Journal of Climate.

Wijngaard, J.B., Tank, A.M.G.K., Können, G.P., 2003. Homogeneity of 20th century European daily temperature and precipitation series. Int. J. Climatol. (ISSN: 1097-0088) 23 (6), 679–692. http://dx.doi.org/10.1002/joc.906, _eprint: https://rmets.onlinelibrary.wiley.com/doi/pdf/10.1002/joc.906.

Wilks, D.S., 1997. Resampling hypothesis tests for autocorrelated fields. J. Clim. 10 (1), 65–82. http://dx.doi.org/10.1175/1520-0442(1997)010<0065:RHTFAF>2.0.CO;2, (ISSN: 0894-8755, 1520-0442). Publisher: American Meteorological Society Section: Journal of Climate.

Wilks, D.S., 2016. "The stippling shows statistically significant grid points": How research results are routinely overstated and overinterpreted, and what to do about it. Bull. Am. Meteorol. Soc. (ISSN: 0003-0007) 97 (12), 2263–2273. http://dx.doi.org/10.1175/BAMS-D-15-00267.1, Publisher: American Meteorological Society.

Wilks, D.S., 2019. Frequentist statistical inference. In: Wilks, D.S. (Ed.), Statistical Methods in the Atmospheric Sciences, fourth ed. Elsevier, ISBN: 978-0-12-815823-4, pp. 143–207. http://dx.doi.org/10.1016/B978-0-12-815823-4.00005-5 (Chapter 5).

Yang, D., Arblaster, J.M., Meehl, G.A., England, M.H., Lim, E.-P., Bates, S., Rosenbloom, N., 2020. Role of tropical variability in driving decadal shifts in the southern hemisphere summertime eddy-driven jet. J. Clim. (ISSN: 0894-8755) 33 (13), 5445–5463. http://dx.doi.org/10.1175/JCLI-D-19-0604.1, Publisher: American Meteorological Society.

Yin, J.H., 2005. A consistent poleward shift of the storm tracks in simulations of 21st century climate. Geophys. Res. Lett. (ISSN: 0094-8276) 32 (18), http://dx.doi.org/10.1029/2005GL023684, Publisher: John Wiley & Sons, Ltd.